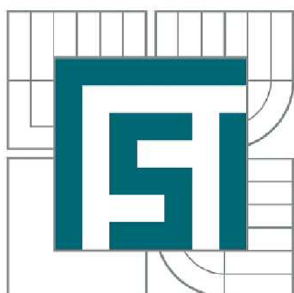# VYSOKÉ UČENÍ TECHNICKÉ V BRNĚ

BRNO UNIVERSITY OF TECHNOLOGY

FAKULTA STROJNÍHO INŽENÝRSTVÍ
ÚSTAV MECHANIKY TĚLES, MECHATRONIKY A BIOMECHANIKY

FACULTY OF MECHANICAL ENGINEERING
INSTITUTE OF SOLID MECHANICS, MECHATRONICS AND BIOMECHANICS

MEMS THERMOELECTRIC GENERATOR FOR AEROSPACE APPLICATIONS

MEMS TERMOELEKTRICKÝ GENERÁTOR V LETECKÉ APLIKACI

DIPLOMOVÁ PRÁCE
MASTER'S THESIS

AUTOR PRÁCE   Bc. LUDĚK JANÁK
AUTHOR

VEDOUCÍ PRÁCE   Ing. ZDENĚK HADAŠ, Ph.D.
SUPERVISOR

BRNO 2014

Vysoké učení technické v Brně, Fakulta strojního inženýrství

Ústav mechaniky těles, mechatroniky a biomechaniky
Akademický rok: 2013/2014

ZADÁNÍ DIPLOMOVÉ PRÁCE

student(ka): Bc. Luděk Janák

který/která studuje v **magisterském navazujícím studijním programu**

obor: **Mechatronika (3906T001)**

Ředitel ústavu Vám v souladu se zákonem č.111/1998 o vysokých školách a se Studijním a zkušebním řádem VUT v Brně určuje následující téma diplomové práce:

MEMS termoelektrický generátor v letecké aplikaci

v anglickém jazyce:

MEMS Thermoelectric Generator for Aerospace Applications

Stručná charakteristika problematiky úkolu:

Diplomová práce si klade za cíl navrhnout autonomní senzorickou jednotku napájenou MEMS termoelektrickým generátorem (MEMS TEG). Napájenou aplikací je snímání (nad)otáček turbíny popřípadě napájení jiné senzorické aplikace (měření teploty, apod.). Cílem práce bude ověření možnosti napájet MEMS termoelektrickým generátorem praktickou aplikaci autonomního snímače s důrazem na letecký průmysl a jeho specifika.

This thesis aims to the research and development of an autonomous sensor unit. The sensor unit will be powered using the MEMS thermoelectric generator (MEMS TEG). The powered application under consideration is the sensing of jet turbine angular velocity and its overspeed. Powering of other suitable applications (e.g. temperature measurements) may be also considered. The main goal of this thesis is the verification of possibilities for powering the autonomous sensor using the MEMS thermoelectric generator. The special attention will be paid to the problems connected with aerospace industry and its specificities.

Cíle diplomové práce:

1. Rešerše dostupných technologií pro leteckou aplikaci autonomního termoelektrického zdroje.
2. Návrh parametrů a vytvoření modelu aplikace autonomního zdroje.
3. Volba elektroniky aplikace autonomního zdroje.
4. Návrh letecké aplikace autonomního zdroje.

1. State of art in field of autonomous thermoelectric generator in aerospace applications.
2. Simulation modelling of this autonomous source of energy.
3. Concept of power management for thermoelectric generator.

4. Design of final autonomous aerospace application.

Seznam odborné literatury:

[1] Goldsmid, H.J.: Introduction to thermoelectricity, Springer, 2010
[2] Rowe, D.M.: Thermoelectrics handbook: macro to nano, Taylor & Francis Group, 2006
[3] Nextreme Thermal Solutions, http://www.nextreme.com

Vedoucí diplomové práce: Ing. Zdeněk Hadaš, Ph.D.

Termín odevzdání diplomové práce je stanoven časovým plánem akademického roku 2013/2014.

V Brně, dne 19.11.2013

L.S.

_____   _____
prof. Ing. Jindřich Petruška, CSc.   prof. RNDr. Miroslav Doupovec, CSc., dr. h. c.
Ředitel ústavu   Děkan fakulty

Abstrakt

Tato diplomová práce se zabývá vývojem autonomního zdroje elektrické energie založeného na MEMS termoelektrickém generátoru. Uvažovaný generátor bude následně použit pro napájení autonomní senzorické jednotky pro letecké aplikace. Systémový pohled na autonomní senzorickou jednotku zahrnuje senzor se zpracováním a přenosem dat, energy harvester (termoelektrický generátor), power management, akumulační prvek a autodiagnostiku. Všechny výše uvedené komponenty jsou v práci podrobně popsány. V úvodu práce je provedena široká rešerše existujících termoelektrických generátorů pro letecké aplikace. Následně jsou popsány základní teoretické poznatky z oblasti DC/DC měničů pro energy harvesting. Zvláštní pozornost je věnována metodám MPPT (Maximum Power Point Tracking). Jako základ pro vývoj napájení autonomní senzorické jednotky bylo provedeno množství simulací za pomoci nástroje MATLAB/Simulink Simscape. Pro identifikaci prametrů modelu posloužilo měření na speciálním přípravku. Praktická implementace teoreticky popsaných problémů je provedena na k tomuto účelu navrženém technologickém demonstrátoru. Závěrem je zhodnocena reálná využitelnost navržené technologie pro finální aplikaci v leteckém průmyslu.

Klíčová slova: termoelektrický generátor, DC/DC měnič, autonomní senzor, energy harvesting, power management, Simscape, MPPT, MEMS, TEG

Abstract

This master's thesis deals with the development of a power source based on the MEMS thermoelectric generator. The proposed power source should be used for supplying of an aircraft-specific autonomous sensor unit. System-level point of view on the autonomous sensor includes the sensor with data acquisition and transmission, energy harvester (thermoelectric generator), power management, energy storage element and self-diagnostics. All the above-mentioned components are described in detail. In the introductory part is provided the broad state-of-art review of aircraft-specific thermoelectric generators. Subsequently are explained the theoretical aspects of DC/DC converters for energy harvesting. The special emphasis is put on the Maximum Power Point Tracking (MPPT). As a basis for the autonomous sensor supply sensor unit design were performed various simulations using MATLAB/Simulink Simscape. The identification of model parameters is based on a measurement with special test bench. The practical implementation of theoretically outlined principles is illustrated on the purpose-designed technology demonstrator. The conclusion deals with an application of the presented technology in an aircraft-specific field and the associated issues.

Keywords: thermoelectric generator, DC/DC converter, autonomous sensor, energy harvesting, power management, Simscape, MPPT, MEMS, TEG

Bibliografická citace:

JANÁK, L. *MEMS termoelektrický generátor v letecké aplikaci.* Brno: Vysoké učení technické v Brně, Fakulta strojního inženýrství, 2014. 81 s. Vedoucí diplomové práce Ing. Zdeněk Hadaš, Ph.D..

Declaration on Word of Honour:

I statutory declare, that I wrote thesis: *MEMS Thermoelectric Generator for Aerospace Applications* by myself and under the supervision of my supervisor.

Brno, 30.05.2014 Luděk Janák

Acknowledgments:

First of all, I would like to thank my supervisor Zdenek Hadas for the enthusiastic guidance and friendly support during the whole masters study period. Our sessions changed my point of view on the academy research and have been a valuable experience for my future career.

I'm grateful for the support given by Division of Aerospace & Advance Control of UNIS, a.s. headed by Vladimir Oplustil. I have had the unique opportunity to reach recent mechatronic technologies in a company environment. My special thanks belongs to my MEMS-TEG-collaborator Zdenek Ancik.

The practical realization of testing procedures would have never been done without the kind help of Ondrej Andrs and Jan Vetiska from my home faculty and Vojtech Vetiska from The Faculty of Electrical Engineering and Communication.

Thus R&D must necessarily be a part of teamwork and dialogue I really appreciated the cooperation with Marian Brazdil from the Energy Institute.

I'm sure that widespread dedications of scientific papers "To my family…" are not heartwarming. So I just want to thank you for everything Barbora, Lojza and Vendula ☺

Last but not least, I'm grateful to my parents for their selfless support during my studies.

Table of Contents

List of Symbols

C_{lp}	[J.kg^{-1}.K^{-1}]	heat capacity of PCM in liquid phase
C_{sp}	[J.kg^{-1}.K^{-1}]	heat capacity of PCM in solid phase
D	[-]	duty cycle
$D_{MPP,boost}$	[-]	duty cycle at maximum power point for a boost converter
$D_{MPP,buck}$	[-]	duty cycle at maximum power point for a buck converter
$D_{MPP,buck\text{-}boost}$	[-]	duty cycle at maximum power point for a buck-boost converter
$D_{MPP,flyback}$	[-]	duty cycle at maximum power point for a flyback converter
f_s	[Hz]	switching frequency
ΔH	[J.kg^{-1}]	heat of phase change
I_{in}	[A] or [mA]	input current
I_{out}	[A] or [mA]	output current
k	[-]	constant
m	[kg]	mass
M_I	[-]	current transfer function
M_U	[-]	voltage transfer function
$M_{U,boost}$	[-]	voltage transfer function of a boost converter
$M_{U,buck}$	[-]	voltage transfer function of a buck converter
$M_{U,buck\text{-}boost}$	[-]	voltage transfer function of a buck-boost converter
$M_{U,flyback}$	[-]	voltage transfer function of a flyback converter
N	[-]	turn ratio
t_{on}	[s]	on-time
t_{off}	[s]	off-time
T	[s]	switching period
T_h	[°C] or [K]	hot-side temperature
T_c	[°C] or [K]	cold-side temperature
T_{JECU}	[°C] or [K]	temperature of JECU
T_{pch}	[°C] or [K]	phase-change temperature
ΔT	[°C] or [K]	temperature difference along the module
ΔT_{peak}	[°C] or [K]	peak temperature difference
P_{el}	[mW]	electric power
$P_{el,\,peak}$	[mW]	peak electric power
$P_{el,\,avg}$	[mW]	average electric power
P_{MPP}	[mW]	output electric power on maximum power point
Q_a	[J]	available heat
Q_c	[W]	heat flow through cold side of thermoelectric module
Q_h	[W]	heat flow through hot side of thermoelectric module
Q_{Ph}	[W]	Peltier cooling on a hot side of TEM
Q_{Pc}	[W]	Peltier cooling on a cold side of TEM
Q_J	[W]	Joule heating

$R_{heatsink}$	[W.K^{-1}]	thermal resistance of heat sink
R_{out}	[Ω]	output resistance
R_{load}	[Ω]	load resistance
R_{in}	[Ω]	input resistance
$R_{install}$	[W.K^{-1}]	thermal resistance of adapters for eTEG HV56
R_{JECU}	[W.K^{-1}]	thermal resistance of path JECU-TEM
R_{TEM}	[Ω]	thermoelectric module internal resistance
Rt_{TEM}	[W.K^{-1}]	thermal resistance of TEM
U_{in}	[V] or [mV]	input voltage
U_{load}	[V] or [mV]	voltage on load
U_{oc}	[V] or [mV]	open-circuit voltage
U_{out}	[V] or [mV]	output voltage
ZT	[-]	figure of merit
λ_{TEM}	[W.K^{-1}]	thermal conductivity of thermoelectric module
η	[-] or [%]	efficiency
$\alpha_{heatsink}$	[W.m^{-2}.K^{-1}]	convective heat transfer coefficient to ambient air
α_{Σ}	[V.K^{-1}]	net Seebeck coefficient

AC	alternating current
APU	auxiliary power unit
ASN	autonomous sensor node
CCM	continuous conduction mode
COTS	commercial-of-the-shelf
DC	direct current
DCM	discontinuous conduction mode
ESR	equivalent series resistance
HUMS	health and usage monitoring system
IC	integrated circuit
JECU	jet engine control unit
LDO	low dropout regulator
MEMS	micro electro-mechanical system
MPPT	maximum power point tracking
NDT	nondestructive testing
NEMS	nano electro-mechanical system
P&O	perturb and observe
PCM	phase change material
PFM	pulse-frequency modulation
PWM	pulse-width modulation
RF	radio frequency
RFID	radio frequency identification
SHM	structure health monitoring

SMPS	switching-mode power supply
TEG	thermoelectric generator
TEM	thermoelectric module
TJ	turbo-jet
TP	turbo-prop
TS	turbo-shaft
ULP	ultra low power
WSN	wireless sensor network

1 Introduction

"It is important to realize that in physics today, we have no knowledge what energy is. We do not have a picture that energy comes in little blobs of a definite amount. It is not that way."
(Richard P. Feynman, 1964)

Despite the fact that our knowledge about energy might be incorrect, we know one certain thing: we can use it and we have to do that.

Systems energy independence is one of the biggest issues connected with energy. Engineers have tried over the centuries to design and build various energy autonomous machines and devices. As a utopian endeavour might be taken a perpetuum mobile while a real-case example is a bicycle dynamo. Nowadays, the energy autonomous systems are of a high interest due to their applications in building control, biomedical implants, automotive and aerospace. All of these applications are mainly electrically powered. Supplying of the energy autonomous systems can be implemented using primary cells or rechargeable batteries. Nevertheless, this approach is disadvantageous as the batteries must be replaced or recharged. Interventions into the system causes additional maintenance and maintenance costs. The system-intervention can be life-threatening in the worst case of biomedical implants. The solution might be find in an energy harvesting - a modern way how to feed the autonomous devices on-site using ambient energy.

The ambient energy sources are represented by vibrations, motion, temperature gradients, light or RF radiation. Thanks to the modern low-power electronics, the small amounts of locally harvested energy are sufficient for powering the wireless sensors, microactuators or any other transducers. Energy harvesting is even more promising in a combination with the micro or nano electromechanical systems (MEMS or NEMS). Energy harvesters are particularly advantageous in the places where is difficult to trace a wiring or where the battery replacement is challenging due to disassemble difficulties.

The presented master's thesis are particularly focused to the field of energy harvesting for supplying autonomous systems in aerospace. Thermoelectric generator based on MEMS thermoelectric module was proposed as a suitable power supply. The considered supplied applications include fully-autonomous sensor and electric power backup for a sensor unit connected to the onboard power distribution of an aircraft. System-level point of view on this energy harvester includes the MEMS thermoelectric module itself, power management, power conditioning, energy storage element, control electronics and self-diagnostics. Above that, an energy harvester is strongly interacting with the supplied load – the low-power system represented by a sensor unit.

Mechatronic design principles along with the model-based design have been employed for the development of a proposed complex harvester. Experiences with the model-based design of energy harvesters have been taken over the long-term research of vibration energy harvesters

at our institution. Simulation modelling have been implemented in MATLAB/Simulink. Practical implementation of the proposed system is illustrated on a purpose-developed technology demonstrator. The presented technology demonstrator was built using the commercial-off-the-shelf (COTS) hardware components whose practical implementability in aerospace should be the task for a further testing procedure. The current results and suggested next steps in the design and development of a reliable thermoelectric harvester for aerospace applications are finally discussed in the conclusion of this thesis.

1.1 Energy Harvesting

Energy harvesting is an art of making useful electric power from ambient energy sources. It's a modern way how to feed the autonomous devices on-site using energy in its surroundings. Promising area for the use of these small amounts of locally harvested energy may be found in the supplying of wireless sensors, temporary testing equipment, biomedical devices, etc. [1], [2]. The energy harvesting approach is particularly advantageous in the places where is difficult to trace a wiring or where the battery replacement is challenging due to disassemble difficulties.

Energy harvesting devices form inherently the complex mechatronic system with all its specificities. Its design should be implemented concurrently with the design of surrounding (superior) systems and should be done with consideration of the surrounding environment. This approach leads to the minimal constrains on the harvester mass, size, and implementation [2].

There are a various suitable phenomena of energy conversion which are useful for an energy harvesting:

- Thermal energy
    - temperature gradients (thermoelectric effect)
    - heat (pyroelectric effect)
    - solar thermoelectrics with focused light (thermoelectric effect)
- Radiant energy
    - optical energy (photovoltaic effect)
    - radiofrequency (RF) energy
    - radioactive energy
- Mechanical energy
    - liquid or gas flow
    - vibrations (piezoelectric effect, electromagnetic, electrostatic)
    - pressure variations (acoustic noise, atmospheric pressure variations)
- Electromagnetic energy
    - Wiegant effect
    - direct electromagnetic energy conversion
- Biochemical energy
    - biochemical fuel cells

Very promising area for utilization of an energy harvesting can be found in a waste heat. Freely available thermal energy sources from chimneys, hot pipes or engines can be recovered using thermoelectric or pyroelectric effects. The thermoelectric effect is the much more efficient one in the terms of Carnot's efficiency. Radiant energy is a very popular method of obtaining electric energy from autonomous device surroundings. Photovoltaic cell forms a part of every calculator while RFID takes a part in every marathon race. Energy of wind and water is commonly utilized using large-scale devices such as wind farms and water power plants. Utilization of flow energy harvesters at the microscale is much more challenging due to the issues connected with withstanding to harsh environments. Nevertheless, some progress in the field of MEMS microturbines have been achieved. Another kinds of mechanical energy harvesting are using "smart" materials such as piezoelectric and dielectric elastomer generators. Free electromagnetic energy is available in the form of oscillating magnetic fields surrounding AC power lines. This energy might be useful for power lines monitoring. Biochemical fuel cells are very promising as the "in vivo" supply for biomedical implants [1]–[3].

Energy harvesting systems generally consist of energy harvesting element, energy storage element and interface power electronics. The harvested power must be converted to electricity and transformed to an appropriate form for charging the energy storage element and supplying the final application. The utilization of special power electronics enables the extraction of maximum available electric power [2], [4].

Each of the energy conversion methods used in an energy harvesting has its own performance characteristics such as power density described by the power-to-weight, power-to-area or power-to-volume ratio. The illustrative example of energy harvesters' power densities is given in Tab. 1. The stated values are describing the overall harvester power density. For instance, the thermoelectric generator power density comprises the heat sink weight and the vibration generator power density comprises the moving mass. The direct comprehension of energy harvesting methods in the terms of power density is misleading. The power density too much depends on the system integration. For instance, the weight of thermoelectric module in Tab. 1 represents only 0.1 % of the whole system mass. The majority of TEG weight is represented by the heat sink. There is a lot of space for the "smart integration" in this field. More comprehensive overview of energy harvesting energy densities could be found in [1]–[4].

Tab. 1 Energy densities of different energy harvesters [5]

Harvester type and operating conditions	*Power density* [mW/kg]
Flexible silicon solar cell inside room or cabin (illuminance: 1000 lx)	9
Flexible silicon solar cell on daylight (illuminance: 10 000 lx)	338
Vibration generator VEH 360 ($a = 0.24$ m/s^2, 60 Hz)	3
Vibration generator VEH 360 ($a = 0.98$ m/s^2, 60 Hz)	42
Thermoelectric generator Eureca TEG1-9.1-9.9-0.8/200 ($\Delta T = 10$K)	10
Thermoelectric generator Eureca TEG1-9.1-9.9-0.8/200 ($\Delta T = 40$K)	34

The two most useful phenomena connected with the aircraft-specific energy harvesting include thermoelectric and electromechanical energy conversion. Thermoelectric devices are advantageous for the applications on fixed-wing aircrafts while electromagnetic transducers are preferable on helicopters with significant low natural frequencies of rotor vibrations [6].

The further work will be focused only into the field of thermoelectric energy harvesting due to their valuable specificities for fixed-wing aircraft applications.

1.2 Motivation for TEG in Aerospace Industry

The aerospace industry is a very specific area of science and technology. The products of aerospace industry are usually designed for a long lifetime and their full functionality is critical. Thus the maintenance consume a significant amount of aircraft operation costs. According to [7], the aircraft maintenance represents the biggest item for airlines, commonly comprising 15–18% of operational expenses. Other expenses comprise mainly of costs for labor and fuel.

The next critical parameter of aircraft systems is their weight. Batteries and wiring take a not negligible amount of aircraft unladen weight. Moreover, the aircraft load is significantly increased by the test equipment during a test flights. Comprehension of the total cable length in typical aircrafts is given in Fig. 1. As the result of these considerations, the most suitable systems for the implementation of thermoelectric energy harvesting include [6]:

- maintenance support;
- cabin crew support;
- flight test instrumentation;
- power supply backup of critical systems.
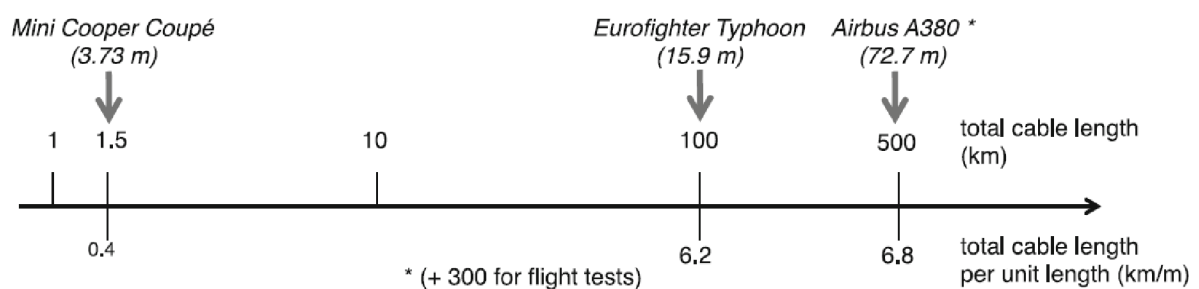
Fig. 1 Cable length comprehension [8]

The utilization of thermoelectric generators in an aerospace industry is usually discussed along with the implementation of wireless sensors networks (WSNs). In the combination with WSNs, energy harvesting using thermoelectrics is one of the very promising emerging technologies associated with structural health monitoring (SHM). Future direct incorporation of smart SHM sensors into the aircraft materials structure is possible [9]. Nowadays, the complicated dismounting of casing, inspections through borescope and damage detection using non-destructive testing techniques (NDT) have to be utilized during the mandatory scheduled checks

of an aircraft. The aircraft checks are always associated with enormous manpower needs. The greatest expectation connected with TEG-supplied WSNs is the step forward from scheduled to predictive maintenance. The predictive maintenance is not driven by strict scheduled time intervals but incorporating the real aircraft state instead. The implementation of TEGs along with WSNs might also be helpful for the cabin crew. The state of seatbelts and the presence of passengers in their seats might be monitored using autonomous sensors. Moreover, the reconfiguration of cabin seating would be possible without any further changes in airplane wiring. The last but not least perspective application is the utilization of TEG as a power supply backup of critical systems. This approach doesn't eliminate the wires but affects positively the aircraft safety and reliability.

The perspective application areas are set. The next logical step is to find the opportune spots for placing TEG on an aircraft. The spots under consideration include engine with its bay, auxiliary power unit (APU), bleed system, electrical and hydraulic actuators, electronic systems, cabin lining and crown of an aircraft. Fig. 2 shows some of these opportune spots [5], [8], [10].
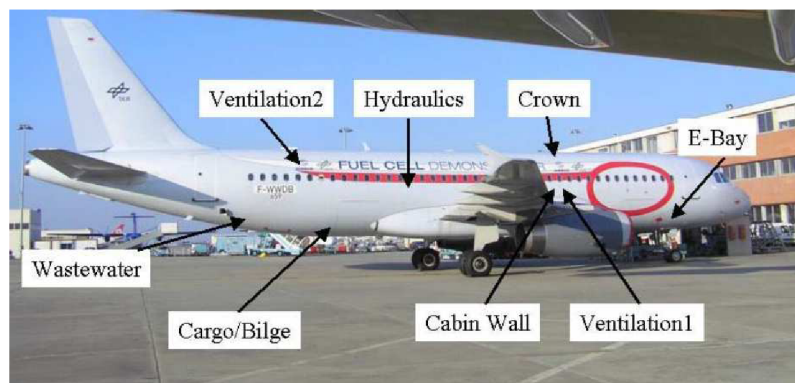
Fig. 2 Opportune spots for placing of TEG on an aircraft [10]

More generally, the thermoelectric generator can be placed in the areas classified as [8]:

- pressurized and temperature controlled zone (aircraft cabin);
- non-pressurized and non-temperature controlled zone (inside the aircraft structure);
- extremely harsh environment (around engine or brake).

Each of the opportune spots on an aircraft can be classified accordingly to the above-mentioned acres. Its placement determines the required specifications. For instance, the thermoelectric generator used for supplying the passenger seat status situated in the aircraft cabin may not necessarily meet that strict regulation as TEG in an engine bay providing the critical sensing tasks for the engine control or protection. Moreover, the thermoelectric generators inside the aircraft cabin may not be tested for the whole aircraft operation envelope insomuch as their temperature is maintained around room temperature. On the other hand, the critical systems for the control and propulsion of an aircraft are placed outside the pressurized and temperature controlled zone. Utilization of TEG into the critical systems requires a reliable long-lasting solution capable to operate within the whole operating envelope of an aircraft.

In Tab. 2 are listed some of the opportune spots from Fig. 2 along with temperature differences and peak/average generated electric power. The stated values are based on a computer simulation. The thermoelectric module under consideration is Micropelt TGP-751. This thermoelectric generator module is based on micro-electro-mechanical-systems (MEMS) technology.

Tab. 2 Opportune spots for placing of TEG on an aircraft – temperature differences and output powers [10]

Spot (cold and hot side)	ΔT_{peak} [°C]	$P_{el, peak}$ [mW]	$P_{el, avg}$ [mW]
cargo skin / cargo primary insulation	40	34.15	22.58
hydraulic pipeline 1 / hydraulic pipeline 2	20	7.97	3.07
waste water tank / waste water ambient	15	5.46	2.99
engine bay fuselage skin / engine bay primary insulation	35	18.72	6.42
cabin wall fuselage skin / cabin wall primary insulation	30	13.36	3.97
cabin wall fuselage skin / cabin wall secondary insulation	40	30.06	11.70

Finally, the basic concept for thermoelectric energy harvesting device for the aircraft-specific purposes has to be chosen. The aircraft-specific thermoelectric harvesting can be principally distinguished between these two areas [6]:

- dynamic thermoelectric energy harvesting (uses temporal temperature variations within the aircraft operation envelope);
- static thermoelectric energy harvesting (uses constant spatial temperature differences).

The dynamic thermoelectric energy harvesting device advantageously uses the temperature changes within the aircraft operating envelope after take-off. Dynamic thermoelectric generator concept is shown in Fig. 3. The temperature difference is formed of a phase-change material (PCM) attached to the thermoelectric generator at the one side and ambient temperature on the other side. The PCM acts as a heat storage. It holds a warm ground temperature accordingly to its heat capacity while the outside ambient temperature decreases. When the heat transmission is over and temperature of the PCM reaches the phase-change temperature, additional heat is produced due to the phase-change of the material. The landing scenario works in vice versa. The PCM is cold while the ambient air is hotter. The phase-change has an opposite direction [7], [11], [12].

All available heat during the dynamic TEG operation can be described as [13]:

$$Q_a = \int_{T_h}^{T_{pch}} mC_{lp}(T)\, dT + m\Delta H + \int_{T_{pch}}^{T_c} mC_{sp}(T)\, dT \qquad \text{(Eq. 1)}$$

where Q_a is the available heat, m the mass of PCM, T_h is the hot-side temperature, T_{pch} is the phase-change temperature, T_c is the cold-side temperature, C_{lp} is the heat capacity of PCM in

liquid phase, ΔH is the latent heat of phase change, C_{sp} is the heat capacity of PCM in solid phase. The corresponding part of Q_a can be transferred to useful electric power using thermoelectric energy conversion.
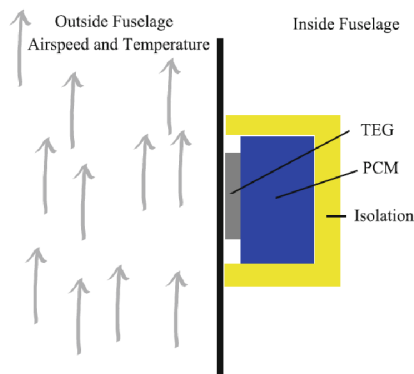
Fig. 3 Practical realization of a dynamic thermoelectric generator – EADS CHOSeN project [7]

The static thermoelectric energy harvesting device uses the constant spatial temperature difference without the "additional heat effect" produced by phase-change material. Static thermoelectric generator concept is shown in Fig. 4. The use of this kind of device is much less popular due to the challenges connected with maintaining the temperature difference along the module. This major challenge is nowadays even more significant along with the MEMS thermoelectric modules. Their hot and cold sides are close to each another (ca. 0.1 mm), thus the thermal isolation between the hot and cold side is complicated. The required size for the heat spreader might be much bigger than in the case of dynamic device [5]. On the other hand, the modern thermal insulation materials along with heat exchange systems such as heat pipes or liquid cooling might be utilized to meet these requirements.
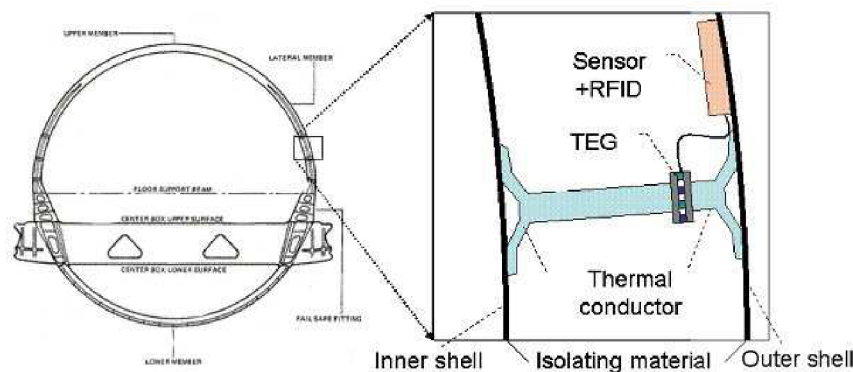
Fig. 4 Practical realization of a static thermoelectric generator – EADS AMETYST project [14]

Thermoelectric energy harvesting is generally very promising for the aeronautic application. However some big issues including the thermal insulation of module sides, withstanding of harsh environments and thermal exchange specificities exist. Aircraft-specific area is very interesting – sonic load in an engine bay, effects of pressure changes, humidity – all of these phenomena affects the heat exchange. Thermoelectric generator thus represents a system strongly interacting with its ambient [8]. Recent solutions are reviewed in the next chapter.

1.3 State of Art

The number of successfully build and laboratory tested thermoelectric generators for aerospace application has increased significantly since the very short review presented in [15]. This chapter gives a brief overview of this research field.

Starting in 2007, the main research activities have been formed around Airbus research facilities (formerly EADS Innovation Works) and cooperating universities. Various designs using a phase-change material prevail. One of the recent prospective applications which is similar to ours jet turbine is the aft fairing thermoelectric generator for powering of ASN. Opportune spot for its placing is shown in Fig. 5. Temperature gradient is provided by the engine waste heat and ambient environment [8].

Fig. 5 Opportune spot for placing of TEG on the pylon fairing of Airbus A380 [13]

Time evolution of the older EADS CHOSeN project can be seen in Fig. 7 – Fig. 9. The thermoelectric generator consisted in the beginning only of containment with phase-change material, commercially achievable TEM and resistive load with measuring equipment. Nowadays, the EADS TEG is retrofitted with special purpose-built power electronics with power management coupled with supercapacitors and thin film batteries. Power density of this particular aircraft-specific TEG is around 4 W/kg [7], [16], [17].
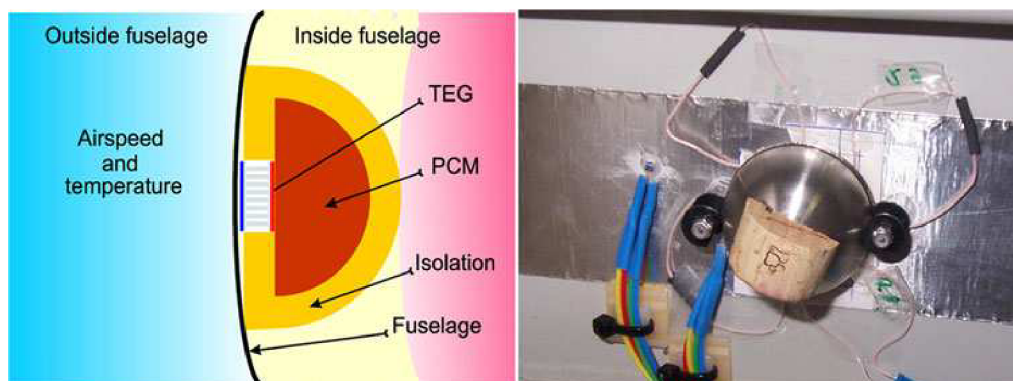
Fig. 6 EADS TEG [18]
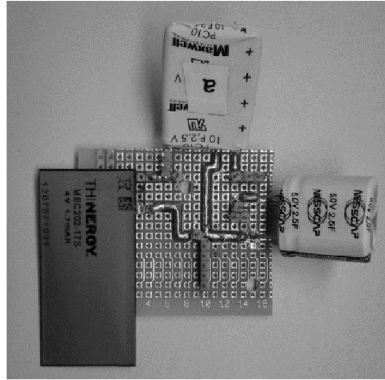
Fig. 7 Combined energy storage unit [17]
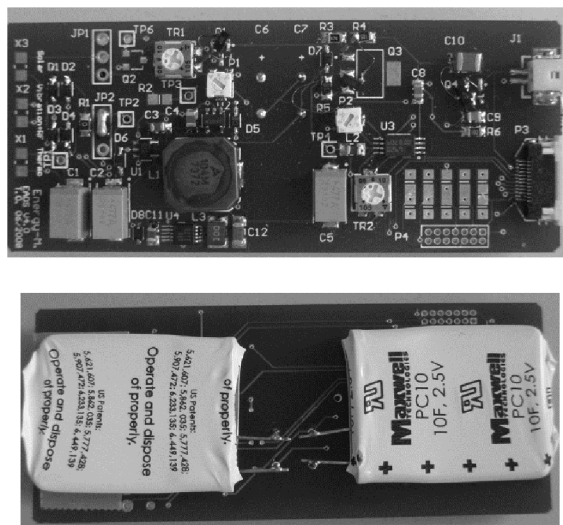
Fig. 8 Aircraft-specific power management electronics for a thermoelectric generator (top: top-side of PCB, bottom: bottom-side of PCB) [5]

The biggest obstacles in the aircraft-specific field are, of course, airworthiness and certification processes. But some progress has been done also in this field. It's notable that above described TEG system built by EADS was successfully tested according to EUROCAE DO-160E avionic test regulations. Random vibration test and thermal cycling test in the temperature range of –65 °C to 125 °C were processed. Function of this energy harvester was also verified during the test flight [16].

All of the reviewed TEG applications in aerospace are mainly focused to the powering of autonomous sensor nodes for the structural health monitoring by the means of energy harvesting. Our proposed application is focused to the new field of power backup for already supplied systems. Such a system is in normal operating states fed from an on-board power distribution bus of an airplane.

2 Problem Definition

"Science is art. It is the process of creating something that never exists before." (Regina E. Dugan)

Aircraft-specific regulations are obsessed with a backup and redundancy of onboard systems. Sensor units placed on an aircraft propulsion system are no exception. Power supplies for these units are a subject of backup and redundancy, hence an unconventional approach to their supplying by electric power is opportune. The main task given to this thesis is a design and development of autonomous sensor unit supplied by the means of thermoelectric energy harvesting. Thermoelectric generator should be based on MEMS technology which was reviewed in the previous work [15]. The autonomous sensor unit should prospectively form a part of the Jet Engine Control Unit (JECU) produced by UNIS a.s [19]. JECU is currently used with the TJ100 engine from První brněnská strojírna Velká Bíteš, a.s [20]. The proposed innovation forms a part of the projects CAAE [21] and ESPOSA [22].

The main tasks given on JECU are engine start-up and stop, acceleration and deceleration and maintenance of turbine angular velocity. JECU is also taking a role of Health and Usage Monitoring System (HUMS) [23]. Reliability of these functions is critical. It's evident, that utilization of TEG into the JECU might be advantageous as a backup for the low-power electronics. An angular velocity sensor was selected as appropriate pilot application. TEG should ensure a continuous electric power delivery in the case of failure in turbine integral generator or onboard power distribution.

The key requirements for the design and development of TEG for aerospace applications based on MEMS thermoelectric module were set as follows:

- supplied system voltage: 3.3 V;
- supplied application power consumption: 100 mW (corresponds to current consumption about 30 mA);
- continuous operation time: 30 min;
- operating temperature range: -50 °C to +85 °C.
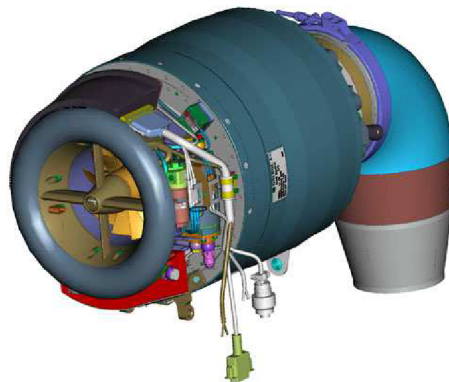
Fig. 9 CAD drawing of TJ100 turbine with JECU (black box in the rear section) [20]

Fig. 10 TJ100 turbine with JECU (black box in the rear section) on the test stand [20]

Above-mentioned requirements might be a subject of further changes. As an instance can be taken the values of supply voltage and current. These values can be decreased assuming the low- or ultra-low-power electronics design.

The hot side of TEG will be placed directly on the surface of JECU. Power electronics inside the package of JECU provide some waste heat which results in the surface temperatures of up to 80 °C. The thermography image of JECU in operation is shown in Fig. 11. The cold side of TEG will be cooled by the ambient air flow. Thus the cold side temperature might be close to the temperature of surrounding environment. The considered location of TEG represents a typical case of static thermoelectric harvesting approach. Sufficient temperature gradient is guaranteed over the dominant part of operating envelope of an aircraft.
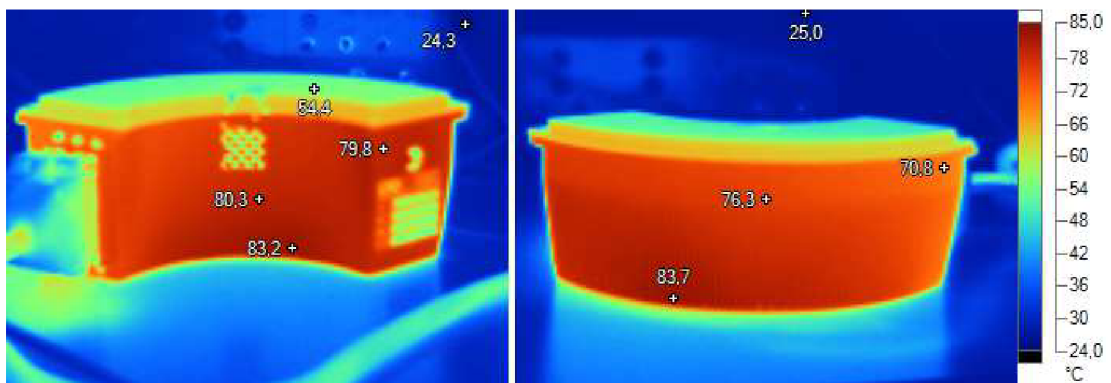
Fig. 11 Thermography image of JECU during its operation under the maximum operating power [24]

Design of a final prototype should be done with the respect to minimal influence of JECU and turbine normal operation. Certification of TEG according to RTCA DO-160/178/254 might be a subject of future demand. Utilization of model-based design principles is a must due to the high complexness of this mechatronic system. Simulation modelling outcomes will be useful for the analogical systems such as waste heat recovery systems and systems for human body energy harvesting. A final product in the scope of this thesis is a technology demonstrator.

2.1 Goals and Objectives

The main goal of this thesis is a contribution to utilization of thermoelectric generators into the aerospace industry. An overall understanding of processes inside thermoelectric energy harvester is a valuable side product. More specifically, the objectives of presented work are:

- to prepare a set of requirements needed for the design and build of the thermoelectric generator for aerospace applications based on MEMS modules;
- to transfer the requirements into preliminary specifications;
- to develop a multipurpose simulation model of thermoelectric generator in MATLAB/Simulink Simscape;
- to prepare an overview of existing COTS solutions in relevant areas;
- to test perspective components;
- to design and build a technology demonstrator;
- to evaluate thermoelectric generators based on MEMS modules for aerospace application purposes;
- to outline a universal methodology for the design and development of thermoelectric generators based on MEMS modules.

Objectives of this thesis are apparently covering only some of the steps in a common scheme of mechatronic design process [25]. The whole development process covered in the presented thesis is depicted in the following simple diagram (Fig. 12).
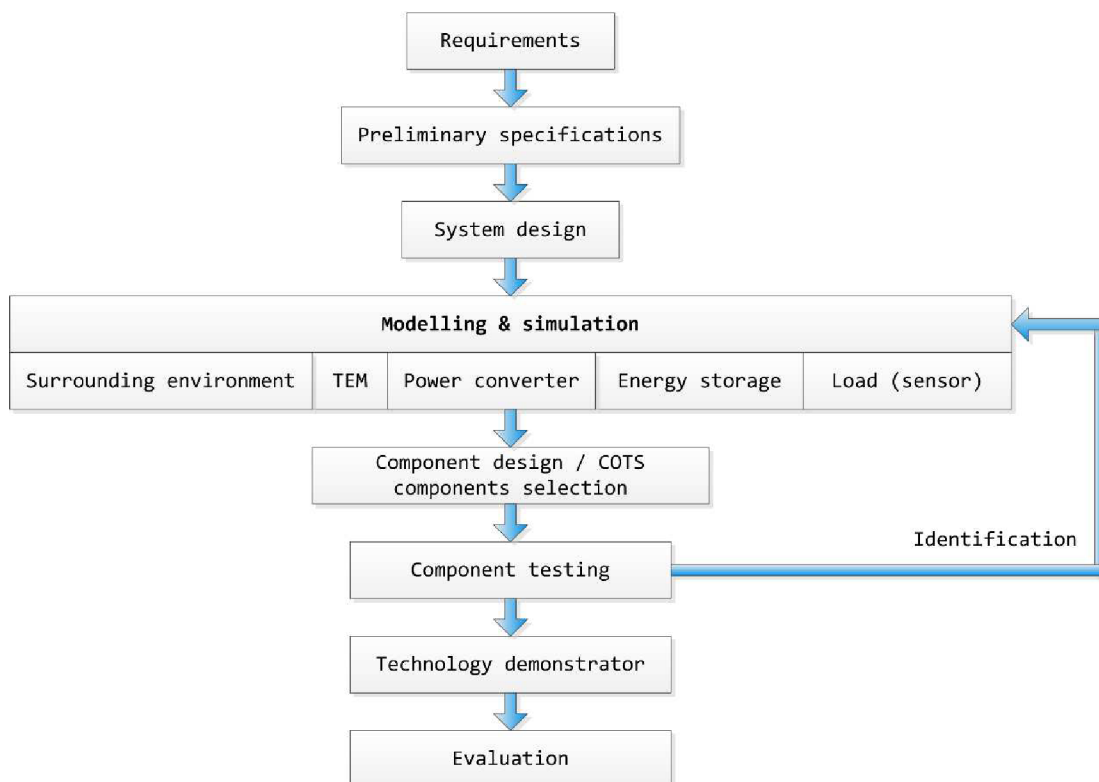
Fig. 12 Diagram of MEMS TEG technology demonstrator development process

3 Theory

"Electrical science has disclosed to us the more intimate relation existing between widely different forces and phenomena and has thus led us to a more complete comprehension of Nature and its many manifestations to our senses." (Nikola Tesla)

3.1 Thermoelectric Energy Conversion

Physical nature of thermal energy harvesting is the Seebeck effect. Its principal is based on the diffusion of electrons through the interface between two different materials. This diffusion is achieved by applying a heating at the junction of two materials which make a thermocouple. Heating causes the net changes in the materials and allows electrons to move from material where they have lower energy into material where the energy of electrons is higher. Because the electrical current is exactly a flow of electrons, this effect of passing electrons from one material to another makes an electromotive force (voltage) across the terminals of thermoelectric module. Generated open circuit voltage is linearly dependent on the temperature difference between hot and cold sides of a thermoelectric module [3], [26]:

$$U_{oc} = \alpha_\Sigma \Delta T \qquad \text{(Eq. 2)}$$

where U_{oc} is the open circuit voltage on the output terminals of the thermoelectric module, S_Σ is the net Seebeck coefficient of TEM and ΔT is the temperature difference along the module ($T_h - T_c$). The net Seebeck coefficient is a characteristic parameter of each TEM.
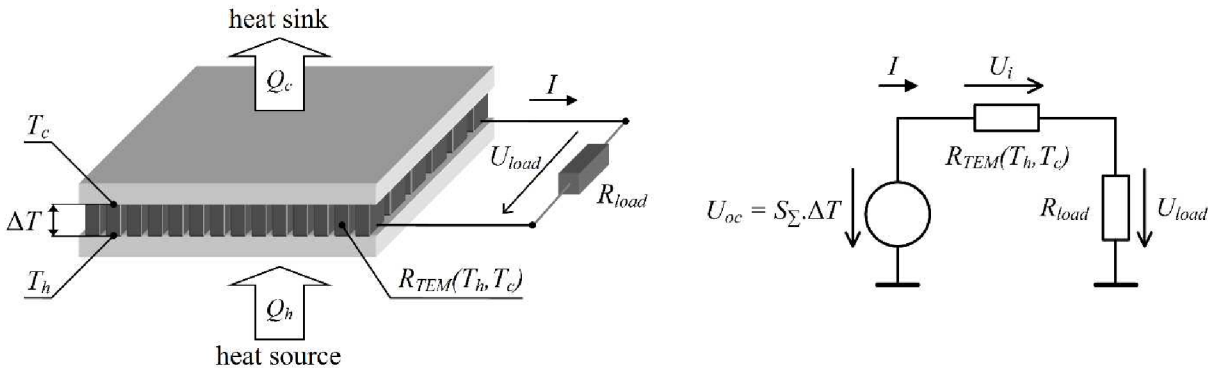
Fig. 13 Thermoelectric module (right) and its equivalent circuit (left)

Much more interesting part of analyses comes up with the connection of TEM into a closed circuit. Situation is depicted in Fig. 13. On the right is depicted the equivalent circuit of TEM in the terms of Thévenin's theorem. Circuit is comprised of an ideal voltage source according to (Eq. 2), TEM internal resistance R_{TEM} and load R_{load}. The output voltage along the load can be actually considered as the output voltage of voltage divider R_{TEM} / R_{load}:

$$U_{load} = \frac{R_{load}}{R_{load} + R_{TEM}} U_{oc} \qquad \text{(Eq. 3)}$$

Thus the power which can be delivered to the load is strictly dependent on the internal resistance of module and resistance of the load connected on its terminals. The maximum power P_{MPP} which can be delivered to the load is [3]:

$$P_{MPP} = \frac{(\alpha_{\Sigma}\Delta T)^2}{4R_{TEM}}$$

(Eq. 4)

This maximum power transfer can be achieved only under the condition:

$$R_{load} = R_{TEM}$$

(Eq. 5)

This state is called the impedance match. Unfortunately, there are practically just a very few supplied applications having their internal resistance matched with energy harvester. Moreover, the internal resistance R_{TEM} is a function of module temperature (T_h, T_c) [27], [28]. Differences between R_{TEM} and R_{load} are usually significant. Dynamic impedance matching is of high interest during the design of power management electronics for an energy harvesting device [3], [4], [6]. The dynamic impedance matching is usually implemented using a switching converter controlled by the Maximum Power Point Tracking (MPPT) driver. Further analyses of the impedance matching for TEG will be provided the cases of boost, buck, buck-boost and flyback DC/DC converters.

As a next challenge, the mechanical installation constraints have to be taken into an account when designing the thermoelectric generator. We will consider our application on JECU as a stationary temperature difference source. This reasoning leads to the major simplifications. It claims, that the temperature difference along the thermoelectric module is the same regardless on the heat flow through the thermal network of TEG. The applications with "soft" temperature difference sources are much more complicated. The temperature difference can rapidly drop down with inappropriate thermal network (heat spreader, heat sink, etc.). An example of such an application are the wearable thermoelectric devices [29]. Moreover, as the thermoelectric generator is a highly complex system, its electric behaviour can be significantly influenced by the thermal constraints. Then the further optimization procedures have to be involved in the solution of an appropriate TEG [30].

An interesting area is the connection of more TEMs into electric circuits. The electric schematic has to be taken into an account when considering the electrically connected non-uniform heated TEMs. Recent investigations shown that a serial connection of TEMs is more advantageous. Parallel or serial-parallel connections lead to parasitic heating of certain TEMs in the circuit. Heating is caused by the Peltier effect and yields in the temperature drop on certain modules. Thus a lower voltage and power is produced [31]. Another solution might be found in the individual module power point tracking. Each individual TEM (or string of TEMs) in such a systems has its own converter. A similar approach is used in photovoltaics. This approach is commonly used on the large arrays of bulk technology TEMs [32], [33].

For the sake of completeness should be mentioned a Carnot's character of the thermoelectric conversion. The maximum theoretic achievable efficiency of the thermoelectric energy conversion is:

$$\eta = \frac{P_{el}}{Q_h}$$

where P_{el} is the electric power delivered to load and Q_h is the heat flux through the hot side of module. The overall performance parameter which couples together the thermal and electric behaviour of thermoelectric module is a device figure-of-merit ZT [27]:

$$ZT = \frac{\alpha_\Sigma^2}{\lambda_{TEM} R_{TEM}} T$$

ZT is a function of the net Seebeck coefficient α_Σ, thermal conductivity of module λ_{TEM} and electric resistance of a module R_{TEM}. The interpretation of this equation results in the need for thermal insulating modules with high Seebeck coefficient and low electric resistance. The higher the ZT is, the better the performances of TEM are. Normal value for commercial MEMS TEMs is around $ZT = 0.75$.

3.2 Load Matching

As was mentioned above, the load (or impedance) matching is of high interest in the power management electronics for energy harvesters. Load matching is usually implemented using the switching mode power supplies (SMPS). Most frequently used topologies of these DC/DC switching converters are [34]:

- boost converter – output voltage is always greater than input voltage;
- buck converter – output voltage is lower than input;
- buck-boost converter – output voltage can be either higher or lower;
- flyback converter – isolated buck-boost converter with transformer at the input;
- (charge pump) – special inductorless case of SMPS, various input/output relations.

The DC/DC converter can be simplified as a two-port network. This approach is depicted in Fig. 14.
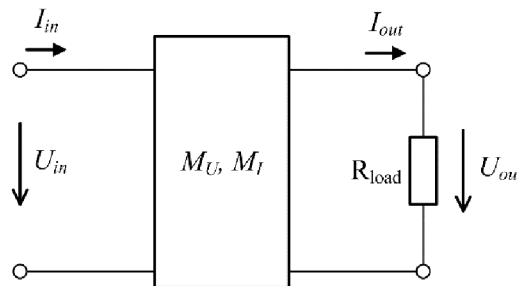
Fig. 14 DC/DC switching converter as a two-port network

According to Fig. 14 can be derived the voltage (M_U) and current (M_I) transfer functions for the two-port network of a converter:

$$M_U = \frac{U_{out}}{U_{in}} \qquad \textit{(Eq. 8)}$$

$$M_I = \frac{I_{out}}{I_{in}} \qquad \textit{(Eq. 9)}$$

$$M_I = \frac{1}{M_U} \qquad \textit{(Eq. 10)}$$

An initial idea of the load matching is adjustment of the converter input resistance according to R_{TEM}. Output and input resistance of such a converter can be expressed as:

$$R_{in} = \frac{U_{in}}{I_{in}} \qquad \textit{(Eq. 11)}$$

$$R_{out} = \frac{U_{out}}{I_{out}} \qquad \textit{(Eq. 12)}$$

which yields in the equation for the input resistance in the terms of output resistance (load):

$$R_{in} = \frac{1}{M_U^2} R_{out} \qquad \textit{(Eq. 13)}$$

Load matching is simply the impedance (resistance) accommodation of output resistance to suitable input resistance. A DC/DC converter works as an impedance adapter. Ratio between the output and input resistance is adjusted using the duty cycle controlled switch. Load matching can be achieved using PWM driver with MPPT control. The pulsed-frequency modulation (PFM) might be considered to minimize the switching loses on low load currents [35]. PFM is usually implemented as a constant on-time or constant of-time controller. Its implementation is of rising interest among the power management circuits for energy harvesting [36]. Several designs combining the PFM and PWM with current threshold have been also introduced [37].

Fig. 15 shows the concept of load matching on specific case of a boost converter. The switching duty cycle D applied on switch S can be expressed as:

$$D = \frac{t_{on}}{T} = \frac{t_{on}}{t_{on}+t_{off}} = f_s t_{on} \qquad \textit{(Eq. 14)}$$

which demonstrates the possibility to control the duty cycle by either PWM or PFM. PWM is ensured by changing the t_{on} while the PFM is implemented by the changes in switching frequency f_s with constant on-time t_{on}.

Transfer functions of M_U, M_I and R_{in}/R_{out} for the most frequently used DC/DC converters in continuous conduction (CCM) mode will be stated in the following chapters. The comprehensive overview of SMPSs can be found in [38].
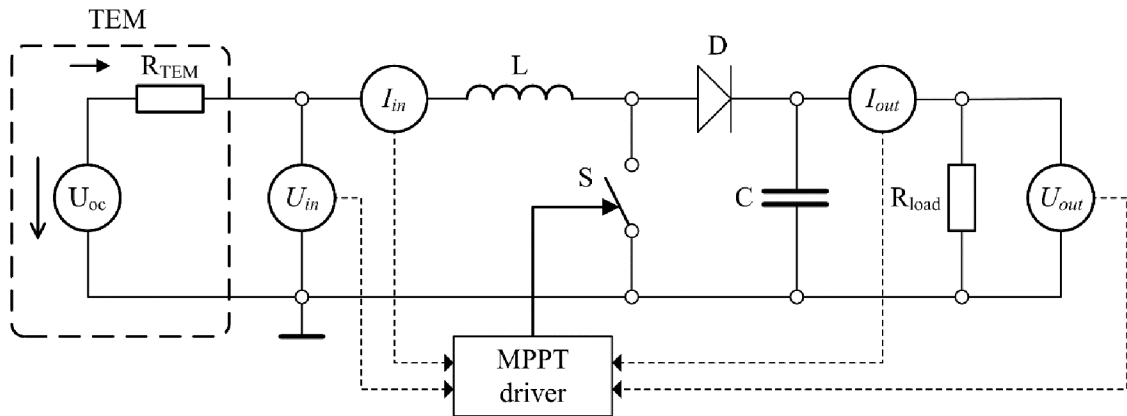
Fig. 15 Concept of load matching (shown on a case of boost-converter)

3.2.1   Boost Converter

The boost converter under consideration is shown in Fig. 16. It is the most important converter topology in energy harvesting as the harvested voltage levels are usually quite low.
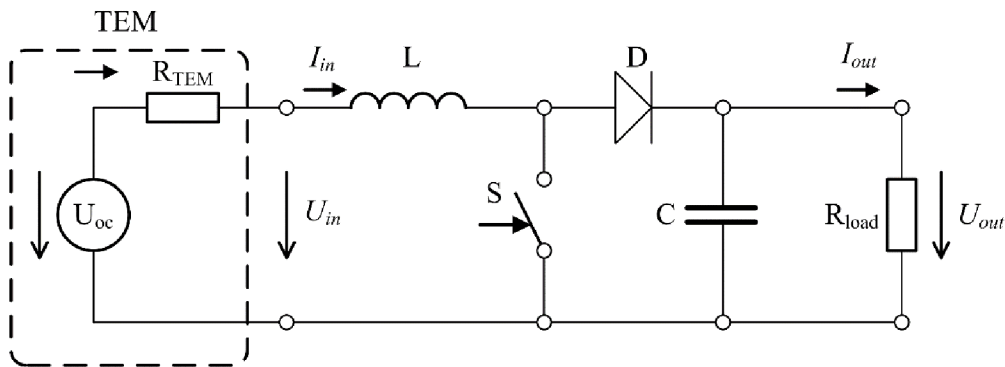
Fig. 16 Boost converter

Voltage and current relations are:

$$M_{U,boost} = \frac{1}{1-D} \qquad\qquad\qquad (Eq.\ 15)$$

$$U_{out} = \frac{1}{1-D} U_{in} \qquad\qquad\qquad (Eq.\ 16)$$

$$I_{out} = (1-D)I_{in} \qquad\qquad\qquad (Eq.\ 17)$$

Combination of Eq. 13-15 yields in the function describing the input/output resistance:

$$R_{in} = (1-D)^2 R_{out} \qquad\qquad\qquad (Eq.\ 18)$$

Duty cycle for the maximum power point condition (Eq. 5) can be expressed as:

$$D_{MPP,boost} = 1 - \sqrt{\frac{R_{TEG}(T_h, T_c)I_{out}}{U_{out}}} \qquad \textit{(Eq. 19)}$$

Note, that the internal resistance of module R_{TEM} is a function of module temperature. Fig. 17 shows the maximum achievable ratios between the output and input voltages with appropriate load and source resistances. A converter is not capable of providing the "unlimited" conversion ratio.
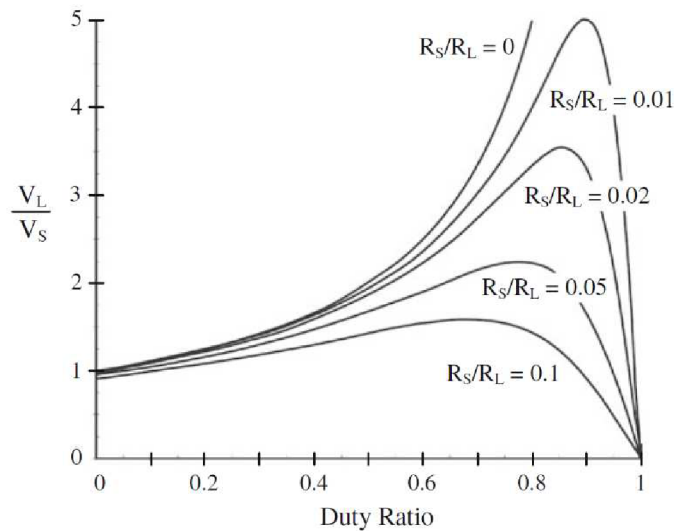
Fig. 17 Output/input voltage as a function of duty cycle for a different relations between source and load resistance when operating the boost converter [39]

3.2.2   Buck Converter

Typical example of a buck converter is shown in Fig. 18. Output voltage of a buck converter is always lower than input. This type of converter is advantageously used in photovoltaic or piezoelectric energy harvesting applications.
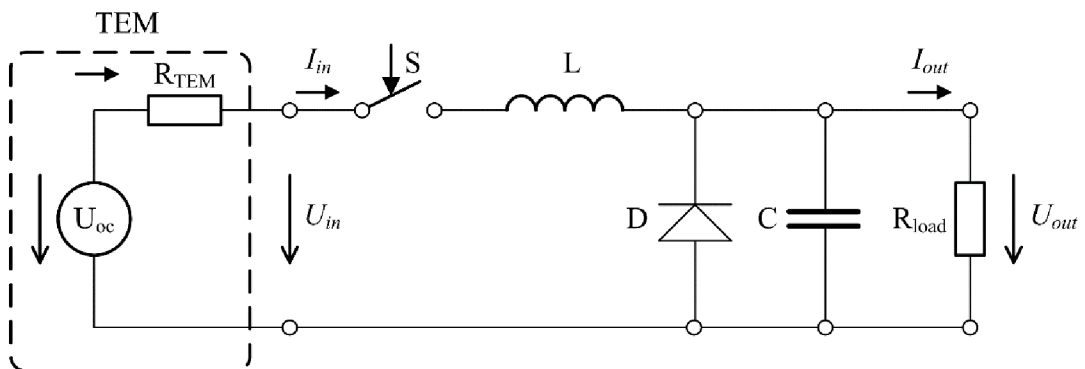
Fig. 18 Buck converter

Functions describing the operation are:

$$M_{U,buck} = D \qquad \textit{(Eq. 20)}$$

$$U_{out} = DU_{in}$$ $$(Eq.\ 21$$

$$I_{out} = \frac{1}{D} I_{in}$$ $$(Eq.\ 22)$$

Desired relation between the input and output resistance can be expressed as:

$$R_{in} = \frac{1}{D^2} R_{out}$$ $$(Eq.\ 23)$$

and a combination with MPP condition yields in:

$$D_{MPP,buck} = \sqrt{\frac{U_{out}}{R_{TEG}(T_h,T_c)I_{out}}}$$ $$(Eq.\ 24)$$

3.2.3   Buck-Boost Converter

Buck-boost converter is widely used and implemented in many commercial integrated circuits for energy harvesting. Its application area covers all the kinds of energy harvesting. Typical example is given in Fig. 19.
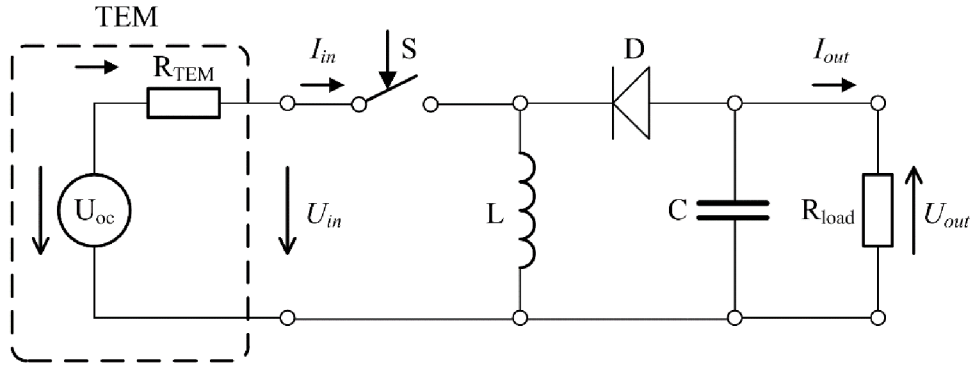
Fig. 19 Buck-Boost converter

Basic voltage and current equations for a buck-boost converter in CCM are:

$$M_{U,buck-boost} = \frac{D}{1-D}$$ $$(Eq.\ 25)$$

$$U_{out} = \frac{D}{1-D} U_{in}$$ $$(Eq.\ 26)$$

$$I_{out} = \frac{1-D}{D} I_{in}$$ $$(Eq.\ 27)$$

Input resistance is:

$$R_{in} = \left(\frac{1-D}{D}\right)^2 R_{out}$$ $$(Eq.\ 28)$$

and the maximum power point is achieved under the duty cycle set according to:

$$D_{MPP,buck-boost} = \frac{1}{1+\sqrt{\frac{R_{TEG}(T_h,T_c)I_{out}}{U_{out}}}}$$

(Eq. 29)

3.2.4 Flyback Converter

Flyback converter is capable of providing the output voltages much higher than input. Its typical application lays in power management for thermoelectric generators operating with very low temperature differences. Input voltages are starting at tens of mV [40], [41]. The control electronics of commercially achievable flyback converters is usually separately supplied using charge pumps which allows these very low start-up voltages. Typical operating scheme is shown in Fig. 20.
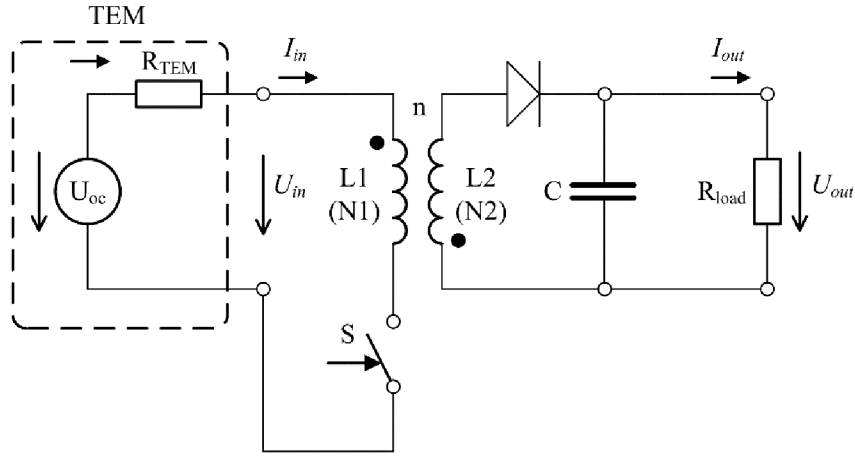
Fig. 20 Flyback converter

Flyback converter has an isolated input ensured by the input transformer with turn ratio *n*. Operation voltages and currents are described as:

$$M_{U,flyback} = \frac{D}{n(1-D)}$$

(Eq. 30)

$$U_{out} = \frac{D}{n(1-D)}$$

(Eq. 31)

$$I_{out} = \frac{n(1-D)}{D} I_{in}$$

(Eq. 32)

which yields in required function for input resistance:

$$R_{in} = \left(\frac{n(1-D)}{D}\right)^2 R_{out}$$

(Eq. 33)

and a maximum power transfer is achieved under the condition:

$$D_{MPP} = \frac{n}{n+\sqrt{\frac{R_{TEG}(T_h,T_c)I_{out}}{U_{out}}}}$$

(Eq. 34)

3.3 Maximum Power Point Tracking (MPPT)

The key problem of load matching is the lack of direct measurement of internal resistance R_{TEM} during the operation. For the maintenance of D_{MPP} belonging to maximum power point can be employed various maximum power point tracking methods. MPPT for applications in thermoelectrics is taken over the established photovoltaic solutions [42]. The most common methods used in recent TEGs are Perturb and Observe (P&O) and Fractional Open-Circuit Voltage (FOCV). FOCV method is periodically disconnecting the TEM from converter. Consequently, an open-circuit voltage on the terminals of TEM is measured. FOCV is based on the observation that MPP voltage can be obtained as a fraction of open circuit voltage:

$$U_{MPP}(U_{oc}) = kU_{oc}$$

(Eq. 35)

Duty cycle is then set to maintain the U_{MPP} input voltage which ensures the maximum power transfer. Typically, $k = 0.5$ is used in the most of TEG applications.

At first are measured values of the input current and voltage which are entering the algorithm. As the next step is computed the exact power on the input terminals of DC/DC converter.

P&O method is perturbing the duty cycle and adjusting its new value based on the measurement of voltage and current on the input terminals of a switching converter. Factually, it's a search for a power maximum in the terms of D. Flowchart of the algorithm is provided in Fig. 21. The biggest disadvantage of this method are the oscillations around the MPP. System is not absolutely stable [39], [42]. It's the most frequently used MPPT algorithm for harvesting higher currents.
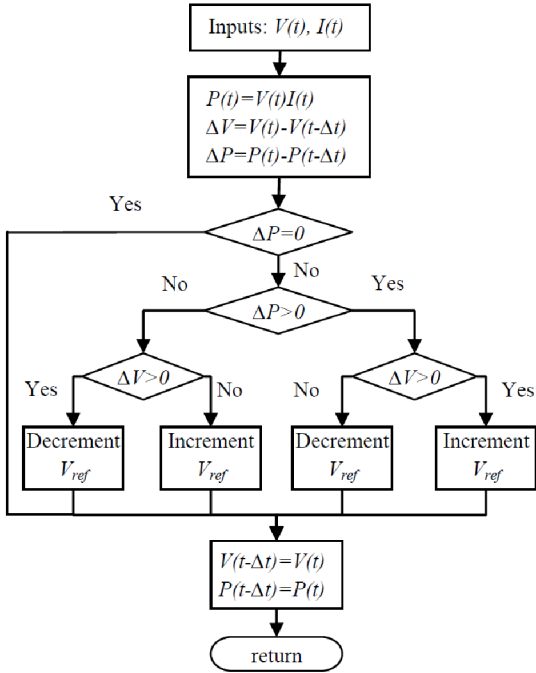
Fig. 21 Flowchart of P&O algorithm [43]

4 Analyses of Existing Solutions

"A good scientist is a person with original ideas. A good engineer is a person who makes a design that works with as few original ideas as possible. There are no prima donnas in engineering." (Freeman Dyson)

The practical design and development of MEMS thermoelectric generator for aerospace applications have started with a necessary technology review and components review. The available commercial-of-the-shelf (COTS) components were selected. The most critical parameters of these components were consequently investigated. Components covered in the overview include thermoelectric modules from the two established MEMS TEM manufacturers – Micropelt GmbH and Laird Technologies (formerly Nextreme Thermal Solutions, Inc.). Various energy storage elements including modern thin-film batteries and supercapacitors are compared. As a base for the development of power management were selected some special purpose integrated circuits.

4.1 MEMS Thermoelectric Modules

There are only a few existing commercially achievable MEMS thermoelectric modules. Micropelt GmbH and Laird Technologies (formerly Nextreme, Inc.) are two rare examples. Two very different thermoelectric modules were chosen for the further experiments. Micropelt TGP-751 is a thin-film generator encapsulated in standard package [44]. See Fig. 22 for disambiguation. This approach ensures an easy manipulation with such a MEMS generator. Dimensions of this thermogenerator-in-package are depicted in Fig. 23. The footprint is around 10x15 mm which guarantee the easy soldering and mounting operations. On the other hand, eTEG HV56 from Nextreme, Inc. is a genuine MEMS [45]. Its footprint is around 3 x 3 mm which makes a manipulation with this device very difficult.

The both electric- end mounting- related parameters are listed in Tab. 3 Comparison of thermoelectric generators suitable for our . Generally, the eTEG HV56 is a harder voltage source with internal resistance around 10 Ω. On the other hand, Micropelt TGP-751 provides the higher output voltages while its internal resistance is much greater (300 Ω).
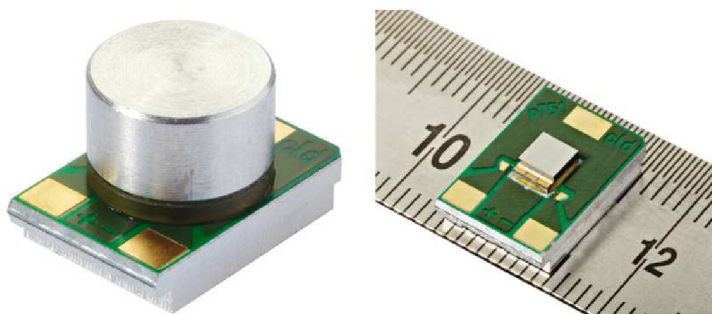
Fig. 22 Micropelt TGP-751 (left: in package, right: with removed package) [44]

Tab. 3 Comparison of thermoelectric generators suitable for our application

	Nextreme eTEG HV56	Micropelt TGP-751
U_{oc} ($\Delta T = 10\ °C$) [V]	0.26	1.25
P_{MPP} ($\Delta T = 10\ °C$) [mW]	1.5	1
U_{MPP} ($\Delta T = 10\ °C$) [V]	0.13	-
I_{MPP} ($\Delta T = 10\ °C$) [mA]	12	-
I_{sc} ($\Delta T = 10\ °C$) [mA]	24	-
Footprint [mm]	3.31 x 3.12	15 x 10
Square area [mm^2]	10.34	150
Thickness [mm]	0.57	9.3
m [g]	-	2.2
T_h [°C]	25 ÷ 200 °C	-
T_c [°C]	0 ÷ 50 °C	-
ΔT [°C]	10 ÷ 200 °C	-
max T_{avg} [°C]	150	100
Operating T [°C]	-	0 ÷ 85 °C
Storage T [°C]	-	-20 ÷ 85 °C
Number of tcs [-]	72	540
$R_{thermal}$ [K/W]	13.1	18
R_{TEM} [Ω]	10.7	250 ÷ 350, ref: 300 (T_{avg}=25 °C)
α_Σ [V/K]	25	110
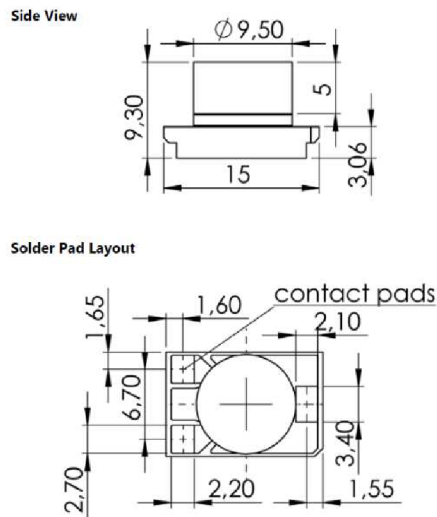
Fig. 23 Micropelt TGP-751 dimensions (in mm) [44]
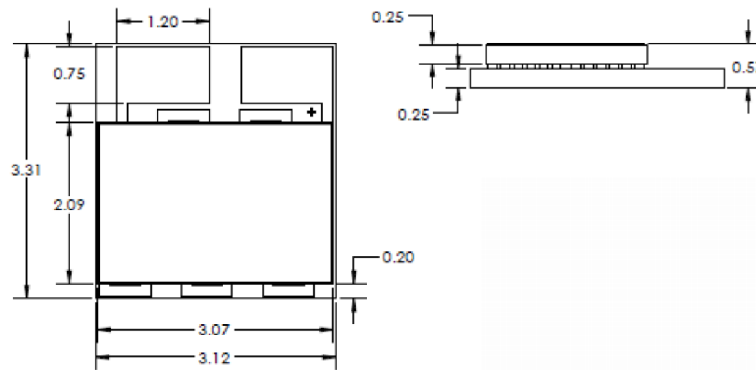
Fig. 24 Nextreme eTEG HV56 dimensions (in mm) [45]

The main reason for the limited commercial market with MEMS TEMs is the length of its research and development process [46]. The way from the new thermoelectric material to the fully-functional module takes at least 5 years. Fig. 25 shows a typical development scheme of commercial thermoelectric generator. The path for a new thin-film TEM is outlined separately.
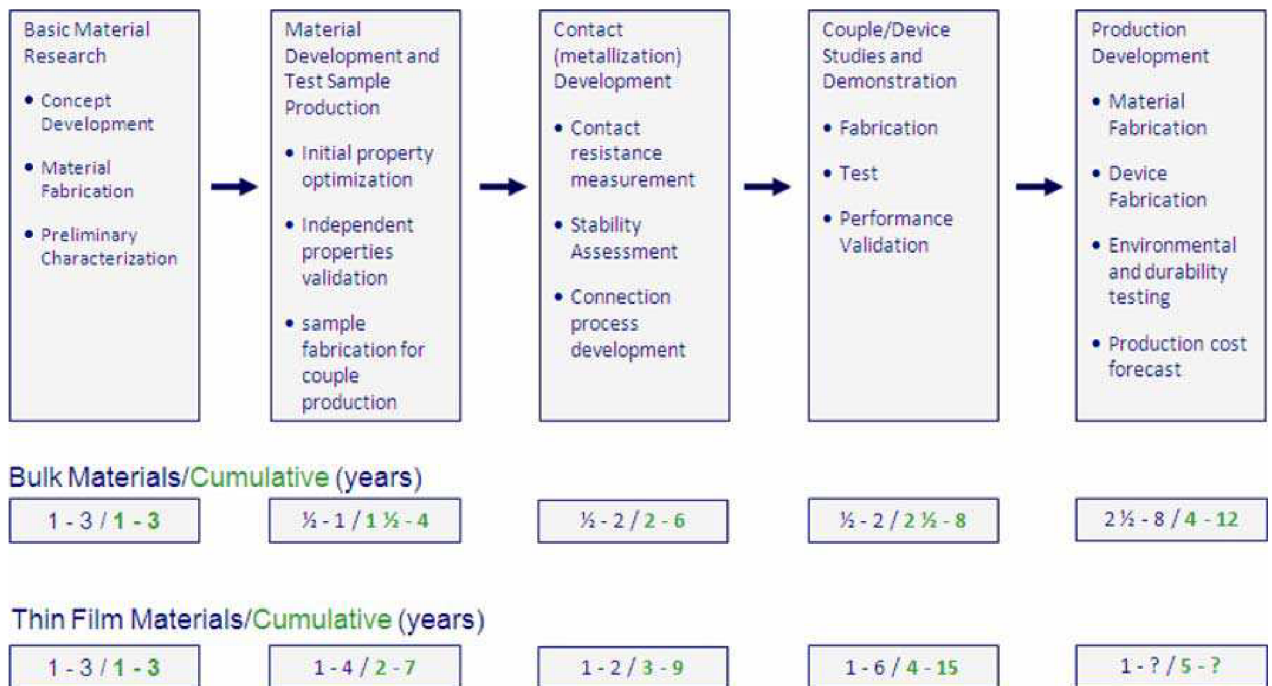
Fig. 25 Typical TEM development scheme [46]

4.2 Electronics

Power management electronics for energy harvesting is usually based on a special switching mode power supplies (SMPS) embedded in purpose-built integrated circuits. These circuits are necessarily equipped with the MPPT control algorithm. Some mature solutions are based on shunt regulators or SMPSs without an MPPT option. As an example may be taken MAX1770 [47] or step-up converter directly embedded into the RF modules from Micropelt GmbH [44].

Hardware implementation of power management electronics for the energy harvesting is of rising interest amongst integrated circuits manufacturers. Various specialized ICs are commercially achievable. The main customer requirements for energy harvesting power management electronics include the Ultra Low Power (ULP) operation, minimum of external components and efficient MPPT algorithm. New trends in ULP electronics replace PWM by the Pulse Frequency Modulation (PFM) for a more efficient operation on low load currents. Key parameters entering the design process are the input/output voltages and currents delivered by TEM and consumed by supplied application.

Tab. 4 sums up the most prospective Ics for our thermoelectric generator. Different Ics are compared in the terms of implemented converter type, MPPT algorithm, input voltage range (U_{in}), output voltage range (U_{out}) and maximum output current ($I_{out,MAX}$). Selected Ics are tailored for the use without an external electromagnetic transformer. An innovative PFM is implemented in Texas Instruments bq25504 [48]. SPV1040T from ST Microelectronics combines P&O algorithm adopted from photovoltaics and requires minimum of external components [49]. SPV1040 is implemented in practical TSOOP8 package. SPV1050 is a brand new buck-boost ULP IC in the stage of prototype [50]. LTC3105 is a long-proven energy harvesting solution from Linear Technology. This integrated circuit enables the connection of external U_{ref} voltage for adjusting the MPP [51]. The above-mentioned integrated circuits are quite simple since their application circuit contains only one inductor. Another opportunity is the use of commercial flyback converters [40], [41] whose applicability is usually advantageous with the very low start-up voltages. For instance, the LT LTC3108 chip provides a start-up option form as low as 20 mV of input voltage. ICs from Linear Technology are usually more complex and provide a various output voltage options including LDOs.

Integrated circuits ST SPV1040T and TI bq25504 were selected for the design and build of a functional technology demonstrator. The selected Ics are implementing a different MPPT algorithm which allows a proper evaluation and final selection of the TEG electronic hardware. The evaluation kit for TI bq25504 was purchased for the further testing procedures.

Tab. 4 Prospective Ics for thermoelectric energy harvesting

	Conv. Type	MPPT	U_{in} [V]	U_{out} [V]	$I_{out,MAX}$ [mA]
TI bq25504	boost	FOCV	0.13-3.0	2.5-5.25	300
ST SPV1040T	boost	P&O	0.3-5.5	2.0-5.2	1800
ST SPV1050	buck-boost	FOCV	0.18-5.3	2.1-5.3	70
LT LTC3105	boost	FOCV	0.25-5.0	1.4-5.0	500
LT LTC3129	buck-boost	FOCV	1.92-15	1.4-15.75	200

4.3 Energy Storage Elements

Energy storage element for aerospace industry has to meet a lot of specific requirements. The main issues are connected with temperature range according to aircraft operation envelope. Another essential think is a long service life. These requirements are met very difficult by the mature battery technology. Overview is presented in Tab. 5. The decision tree when considering a new energy storage element for an aircraft application can be seen in Fig. 26.
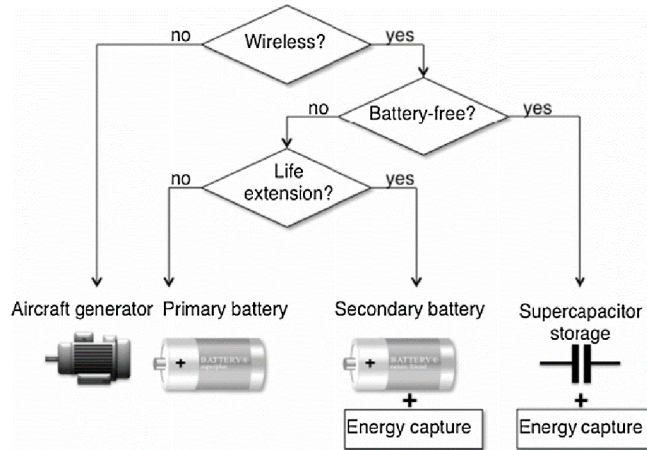
Fig. 26 Decision tree when considering a new aircraft-specific storage element [8]

The new promising technology are supercapacitors or ultracapacitors [17], [52]–[54]. It's still a new technology suffering for the low energy densities. On the other hand the extensions in lifetime and applicable operation temperatures are significant. The tiny thin-film batteries which can be directly embedded into chips on a wafer create a special instance of energy storage elements. Their classification is somewhere between supercapacitors and classic chemical batteries. Their use is especially advantageous in the combination with ULP electronics. Relatively high internal resistance (tens of Ω) is a special feature of thin-film batteries.
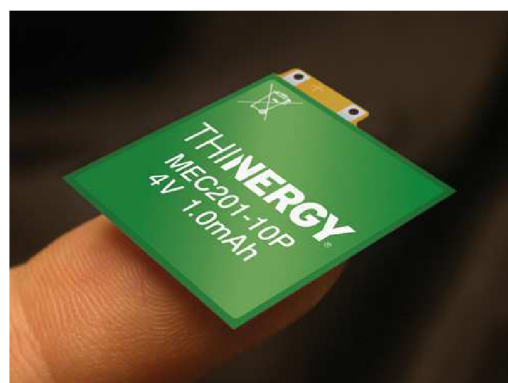
Fig. 27 THINERGY thin-film battery [55]

The mature electric energy storage technologies have not been considered for our application. Their main disadvantages include the blocking effects at low temperatures as well as troubles under the high temperature conditions.

Tab. 5 Comparison of various energy storage elements

Energy storage principle	Rated (cell) voltage [V]	Energy density [Wh/kg]	Capacity [Ah] or [F]	Number of charging cycles	Operation temperature [°C]
NiMH	1,2	80	0,01 – 10 Ah	max. 1000	5 °C – 45 °C
Li-Ion	3,7	200 – 500	0,1 – 10 Ah	max. 1200	-10 °C – 45 °C
Li-Pol	3,7	300 – 400	0,1 – 5 Ah	min. 1200	-10 °C – 45 °C
Supercapacitor	2,5/3,5	5 – 6	0,1 – 100 F	1 000 000	-40 °C – 85 °C
Thin-film bat.	4	550	0,1 – 5 mAh	10 000	-40 °C – 85 °C

Supercapacitors are recently produced by a lot of established component manufacturers. Companies such as AVX, Maxwell Technologies, Celery, Cooper Bussman, Panasonic, WIMA or Kemet produce a broad variety of supercapactiors. Some of them are classified as "extended temperature range"

Fig. 28 AVX BestCap series

The main problem with the temperature changes over the operation range lies in the corresponding changes of internal resistance of the supercapacitor. Typical characteristics of Maxwell supercapacitors over the temperature range are depicted in Fig. 29. Nevertheless, the characteristics vary with temperature, the biggest advantage of supercapacitor is the low freezing point of the organic electrolyte. This feature prevents the damage on low operating temperatures.

Performance vs. Temperature
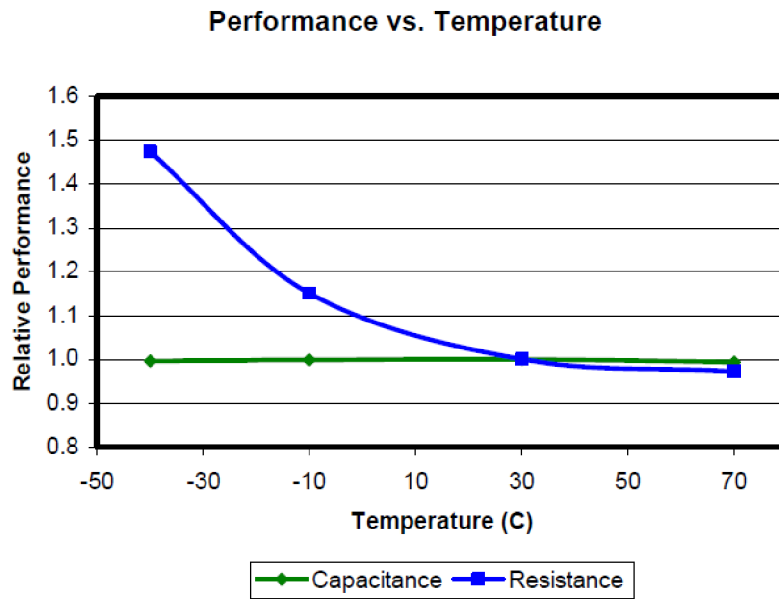
Fig. 29 Increase of internal resistance with low temperatures for a supercapacitor [53]
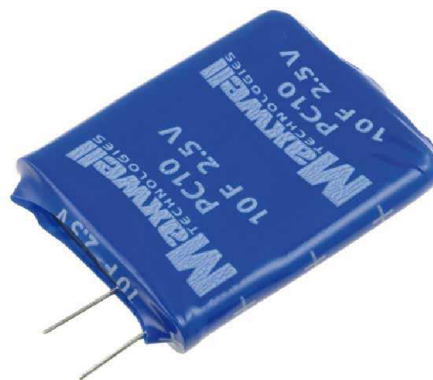
Fig. 30 10F supercapacitor by Maxwell

As an appropriate solution for our application were selected the AVX BestCap ultra-low ESR supercapacitors. Their capacitance is up to 1 F. AVX provides these ultracapacitors in attractive packages as mentioned in Fig. 28. Interesting for further testing would be also the 10F PC-series ultracapacitors from Maxwell. Manufacturer provides also the extended temperature range versions applicable in aerospace industry. The extended temperature lays in the span -40 ÷ +85 °C [54].

5 Experiment

"With engineering, I view this year's failure as next year's opportunity to try it again. Failures are not something to be avoided. You want to have them happen as quickly as you can so you can make progress rapidly." (Gordon Moore)

Inasmuch as the data about MEMS TEMs provided by manufacturers are very poor, the development of custom testing procedures for evaluation purposes is essential. Applications of COTS components in aircraft industry require a much broader spectrum of testing procedures than industrial applications. Characteristics of electrical components strongly varies with temperature, pressure or humidity. MEMS thermoelectric modules are no exception.

A representative set of measurements was proposed for the first stage of MEMS TEM tests. The main purpose of this first stage is the verification of derived models and verification of datasheet information provided by manufacturers. Necessary step is also the evaluation of MEMS TEM devices for their further aircraft-specific application. The whole testing and measurement process was extremely valuable for further considerations about MEMS TEMs manipulation, mounting and durability.

5.1 Measurement Setup

Thus the real testing conditions are very often poorly described in manufacturers' datasheets, the special test bench was prepared for the testing procedures under the controlled conditions. Schematic view of measurement setup is given in Fig. 31. The special test bench with MEMS TEM is placed inside the climatic chamber. The cold-side temperature T_c was controlled by the climatic chamber cooling circuit. The entire test bench is chilled out down to desired T_c until its stabilization. The AC power supply is subsequently turned on which began warming the hot-side of module T_h through the 50 W resistive heating element. Once the hot-side temperature reaches the desired value, the data set is acquired. The temperature feedback is provided by the Pt100 sensors connected to PC via datalogger. Electrical characteristics were measured using precise laboratory multimeters. All the used instruments are listed in Tab. 6.

Tab. 6 Measuring instruments

Designation	Type
Climatic chamber	WEISS WKL100
Pt100 datalogger	OMEGA OM-CP-OCTRTD (8 Channel RTD temperature recorder)
V/A/Ω/Ω_1	Agilent 34401A (6 1/2 digit multimeter)
Ω_2	FLUKE 175 (True RMS multimeter)
AC power supply	Diametral AC250K1D (isolation transformer, 0-255V/1A)
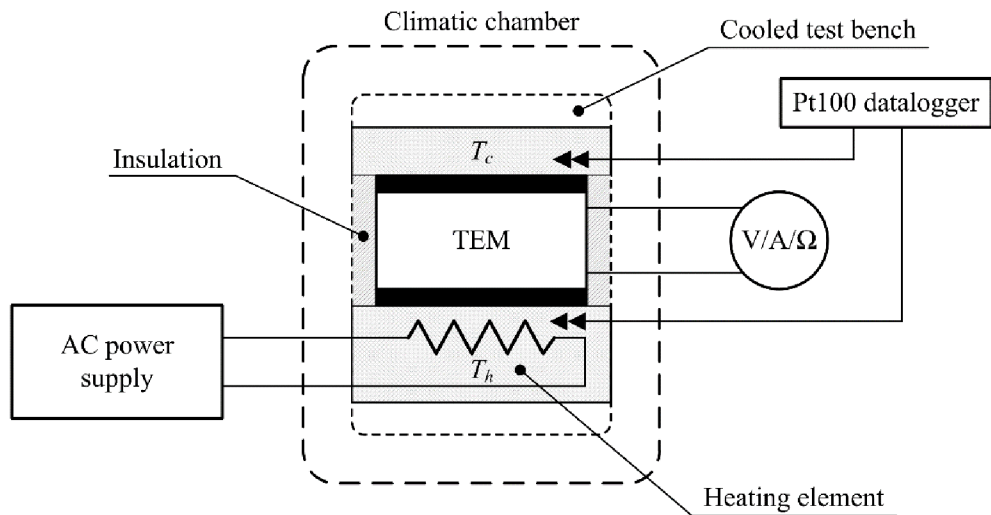
Fig. 31 Measurement setup

A 3D drawing of the test bench internal structure is depicted in Fig. 32. The whole structure is encapsulated in a milled plastic box. Hot side of the module is heated up using a 50 W resistive heater. Thermal insulation between hot and cold sides is ensured by a mineral wool. Aluminium plates are used as heat spreaders. Pt100 sensors are placed in the milled slots as close as possible to the measured TEM. Fig. 33 and Fig. 34 show a various customizations of TEM installation inside the test bench. Each of measured TEMs (Micropelt TGP-751, Nextreme eTEG HV56) needed a specific adjustments in an inside structure of the test bench. The test bench inside the climatic chamber is depicted in Fig. 35. The contact pressure on TEM is ensured by the central screw. Contact pressure can be easily adjusted using a torque screwdriver.
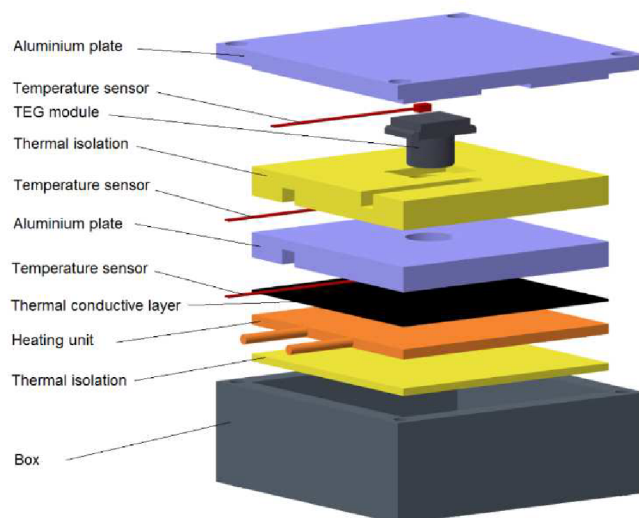
Fig. 32 3D drawing of test bench internal structure [56]
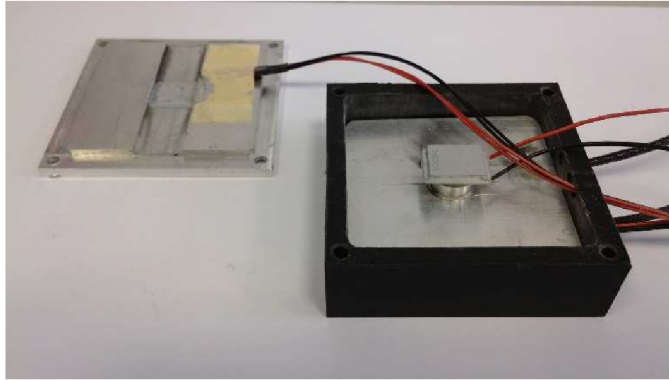
Fig. 33 Test bench for Micropelt TGP-751
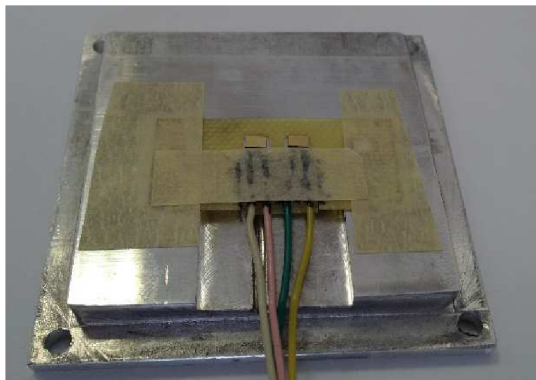
Fig. 34 Test bench for Nextreme eTEG HV56
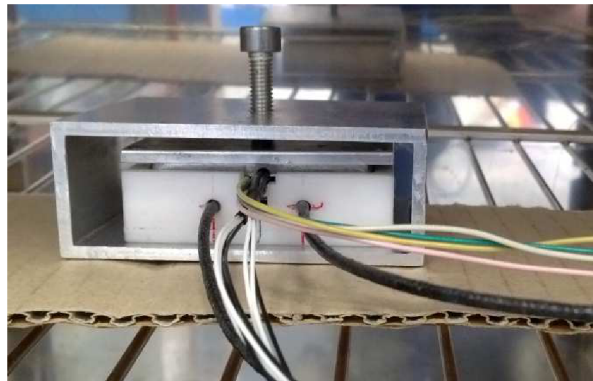
Fig. 35 Test bench inside the climatic chamber

The first verification tests of installation concept were performed after the test bench assembly. Unfortunately, the Micropelt eTEG HV56 tests failed in their beginning. The test bench wasn't capable of providing the sufficient temperature difference along eTEG HV56 module. Thermal insulation of both sides of TEM is quite complicated due to the tiny thickness of module. Tests described in 5.2, 5.3 and 5.6 were carried out with Micropelt TGP-751 only. Moreover, some of the eTEG HV56 modules were damaged during the soldering, installation or dismantling. Their dimensions (ca. 3x3x0.6 mm) are too tiny for a conventional manipulation.

5.2 Open-circuit Voltage Measurement

The open circuit measurement was carried out using a simple method shown in Fig. 36. The linear characteristics of open-circuit voltage U_{oc} in the terms of temperature difference ΔT was obtained. This trend perfectly matches the theory of thermoelectric Seebeck effect described in Eq.2. On the other hand, when comparing the results with datasheet values, the slope of the U_{oc} characteristics is more gradual. This can be caused by the incorrect data from manufacturer or more probably by the inappropriate placing of Pt100 sensor. See appendix for the exact measured values and measurement conditions.
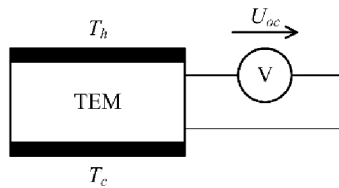
Fig. 36 Open-circuit voltage measurement setup
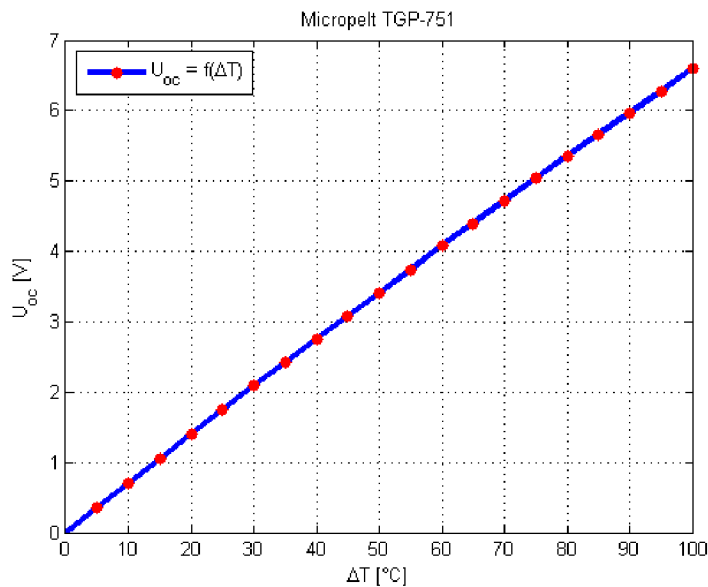
Fig. 37 Open-circuit voltage measurement results (Micropelt TGP-751, ΔT = 0-100°C)

5.3 Short-circuit Current Measurement

The short circuit measurement was carried out using a simple method shown in Fig. 38. The linear characteristics of short-circuit current I_{sc} in the terms of temperature difference ΔT was obtained. The measured data are plotted in Fig. 39. Small disturbances between the linear fit and measuring points are caused by the specific behaviour of Micropelt TGP-751 TEM. While short-circuited, TGP-751 varies in its internal resistance. Some settling time is needed to measure the exact value. The results of short-circuit current measurement satisfactorily match

the expected linear behaviour. See appendix for the exact measured values and measurement conditions.
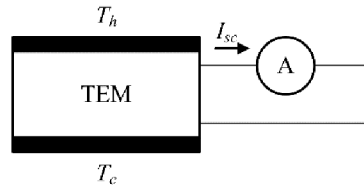
Fig. 38 Short-circuit current measurement setup
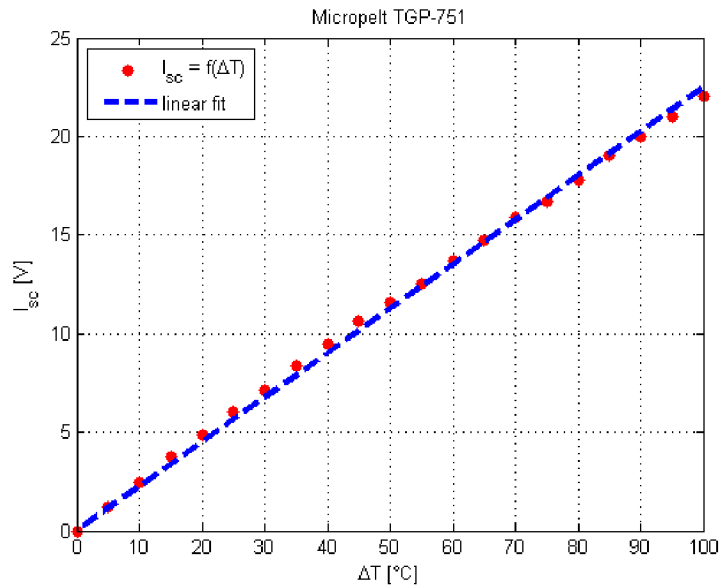
Fig. 39 Short-circuit current measurement results (Micropelt TGP-751, ΔT = 0-100°C)

5.4 Internal Resistance Measurement

The internal resistance measurement was performed concurrently on the both different thermoelectric modules (eTEG HV56, TGP-751). The temperature measurement was acquired by the Pt100 sensor placed close to both of the modules. R_{TEM} temperature characteristics were examined in the temperature span of 200 °C. From -50 to +150 °C. This temperature span is much broader than the one guaranteed by TEM manufacturers. Manufacturers declare in their datasheets quite narrow operating temperature ranges [44], [45]. Measurement setup is depicted in Fig. 40. Measurement results for Nextreme eTEG HV56 are depicted in Fig. 41. Results for Micropelt TGP-751 are following in Fig. 42. See appendix for the exact measured values and measurement conditions. This measurement will be used as an essential input parameter to the model. Its value could be never determined without this measurement (manufacturers guard such a data). Validity of R_{TEM} measurement can't be verified due to the unknown material properties of the modules.
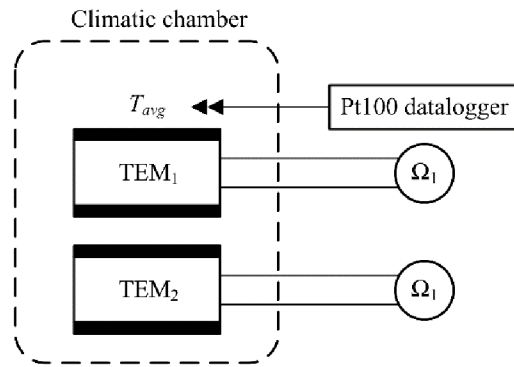
Fig. 40 Internal resistance R_{TEM} measurement setup
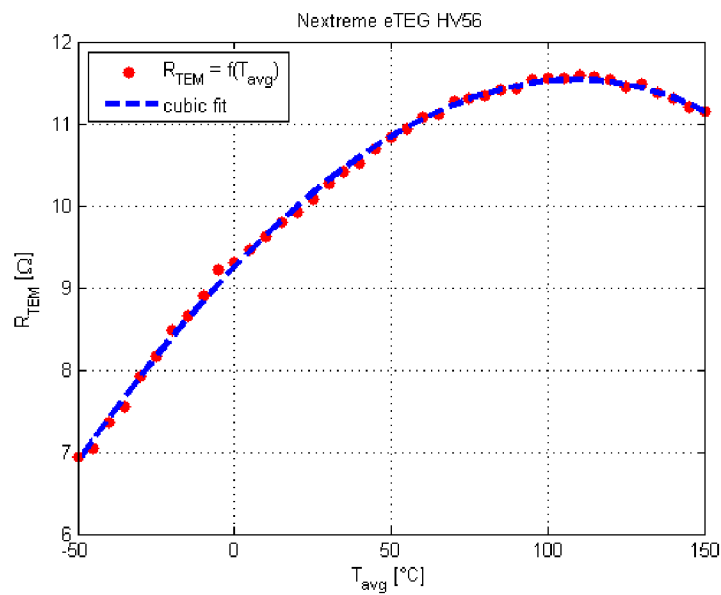
Fig. 41 Internal resistance measurement results (Nextreme eTEG HV56, $T_{avg} = -50 \div +150°C$)
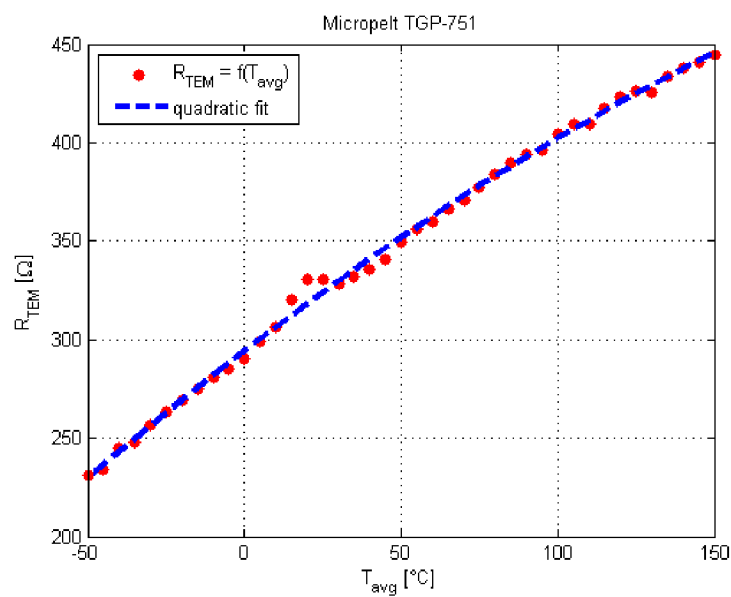
Fig. 42 Internal resistance measurement results (Micropelt TGP-751, $T_{avg} = -50 \div +150°C$)

5.5 Seebeck Coefficient Measurement

The measurement of Seebeck coefficient has only an indicative character. Exact measurements of Seebeck coefficient require a well stabilised temperature source with minimal changes in $\varDelta T$. Therefore, this measurement is impractical with our test bench. The acquired data are listed in Tab. 7 and plotted in Fig. 44. The three measured values have an unequal distribution of the test average temperature T_{avg}. Some variations of Seebeck coefficient can be observed. This knowledge will lead to the design of a new testing procedure for the exploration of MEMS TEM characteristics.
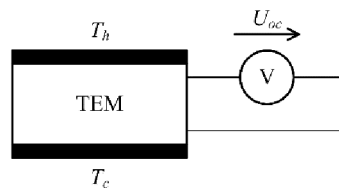
Fig. 43 Seebeck coefficient measurement setup

Tab. 7 Seebeck coefficient variations

T_{avg} [°C]	α_{Σ} [V/°C]	U_{oc} [V]	$\varDelta T$ [°C]	T_h [°C]	T_c [°C]
-27.5	0.059	0.588	10.0	-22.5	-32.5
18.5	0.070	0.35	5.0	21	16
97.0	0.074	1.031	14.0	104.0	90.0
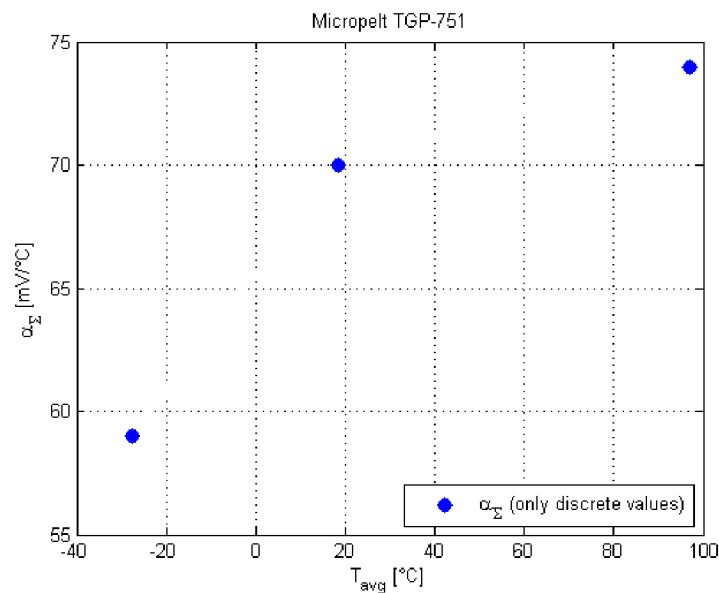
Fig. 44 Discrete plot of Seebeck coefficient variations with T_{avg} (Micropelt TGP-751)

5.6 Calculated Characteristics

Sections 5.2 – 5.6 present the directly measured variables. Their processing results in another interesting findings. The MPP power provided by TEM can be derived as a function of open-circuit voltage and short-circuit current:

$$P_{MPP} = \frac{1}{4} U_{oc} I_{sc}$$

this equation is valid for an electric power source with linear V-A curve. Results of this computation method for P_{MPP} are shown in Fig. 45. The P_{MPP} computed using Eq. 4 is plotted subsequently. As a reference can be taken the blue curve (R_{TEM}-based), since the red one (I_{sc}-based) is influenced by the error described in 5.3.
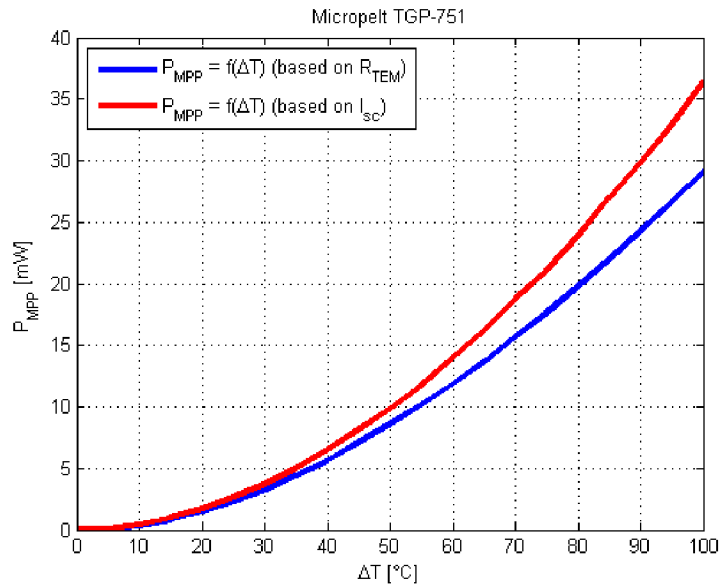
Fig. 45 Power on MPP (Micropelt TGP-751, ΔT = 0-100°C)

Assuming that TEM is a temperature-difference-controlled voltage source with internal resistance R_{TEM}, the V-A characteristics describing its load capability is expressed as:

$$U = U_{oc} - R_{TEM} I$$

Plot of this characteristics for three particular temperature differences is provided in Fig. 46.
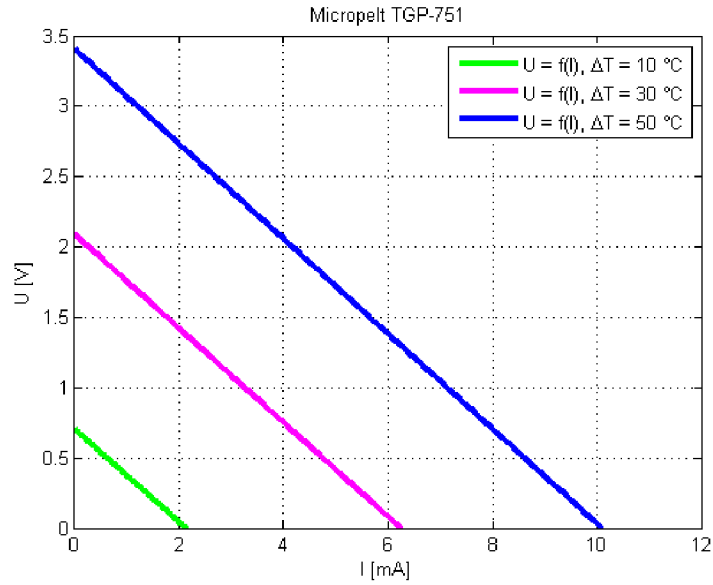
Fig. 46 V-A characteristics comparison (Micropelt TGP-751, ΔT = 10, 30, 50°C)

The power to current characteristics (denoted as W-A) yields in integral of V-I characteristics according to current:

$$P = U_{oc}I - R_{TEM}I^2$$

The obtained parabolic dependency is plotted in Fig. 47. Shape of the W-A characteristics has an appropriate form for the voltage source with linear internal resistance R_{TEM}.
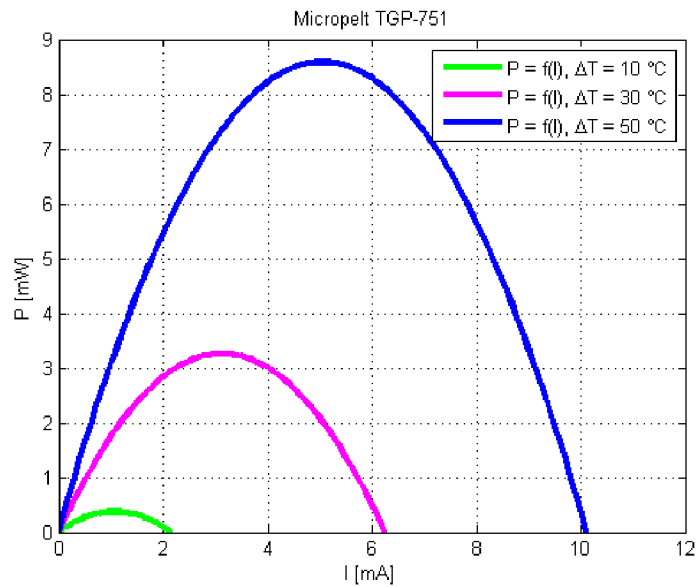
Fig. 47 W-A characteristics comparison (Micropelt TGP-751, ΔT = 10, 30, 50°C)

5.7 Comparison of MEMS Thermoelectric Modules

The older data achieved in [15] were used as a reference values for the Nextreme eTEG HV56 module. The empirical functions describing the open circuit voltage and power output on MPP for eTEG HV56 are given as:

$$U_{oc} = 0.0194\Delta T \qquad \text{(Eq. 39)}$$

$$P_{MPP} = 0.0097(\Delta T)^2 + 0.0632\Delta T \qquad \text{(Eq. 40)}$$

These empirical functions will be further used for comparison of TEMs. Fig. 48 shows the open-circuit voltage for both compared modules. As could be easily seen, Micropelt TGP-751 provides much steeper slope of open-circuit voltage with temperature. This result was expected due to the higher number of thermocouples integrated in TGP-751. Open-circuit voltage is a product of Seebeck coefficient, number of thermocouples and temperature difference along the module.
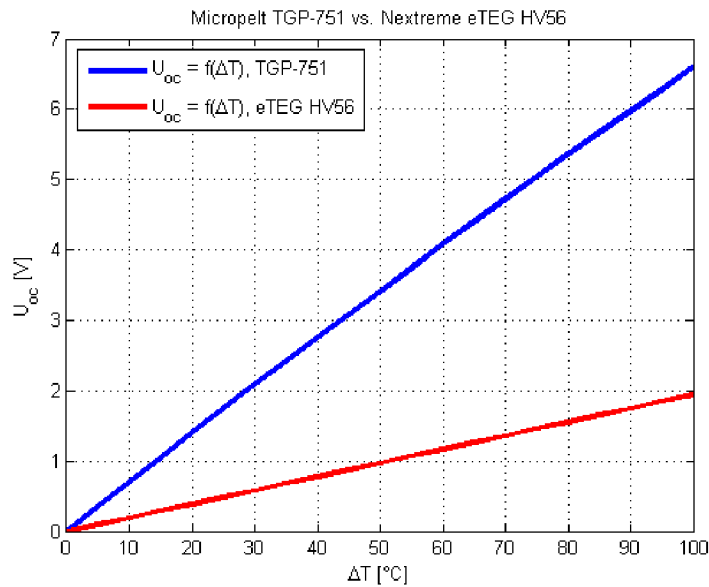
Fig. 48 Open-circuit voltage comparison (Micropelt TGP-751 vs. Nextreme eTEG HV56, ΔT = 0-100°C)

The following characteristics are the domain of Nextreme eTEG HV56. As depicted in Fig. 49, the module is capable of providing four time higher power when operating on its maximum power point. This significant difference is caused by the internal structure of both modules. HV56 is tailored for a high power on MPP (low internal resistance) while TGP-751 aims to the maximum possible voltage (high resistance and net seebeck coefficient).
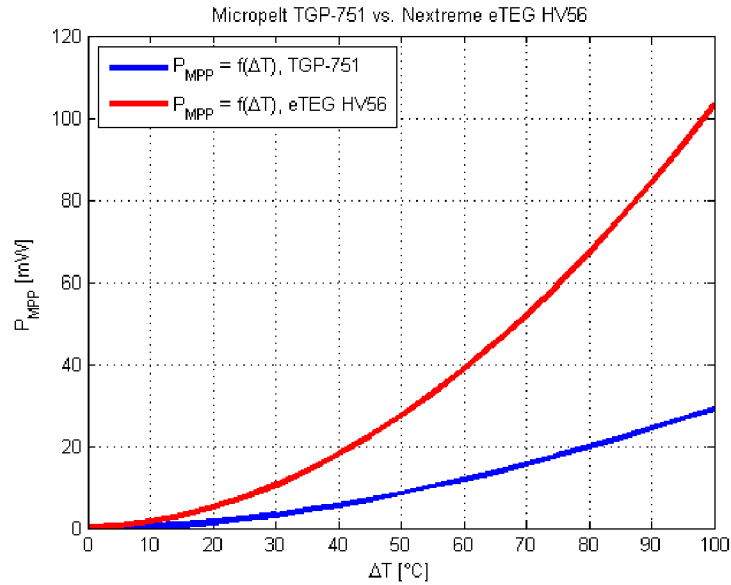
Fig. 49 Power on MPP comparison (Micropelt TGP-751 vs. Nextreme eTEG HV56, ΔT = 0-100°C)

The above-mentioned specificity of both modules is additionally depicted in V-A characteristics in Fig. 50. TGP-751 has a steep characteristics while eTEG HV56 drops down much more gradually.
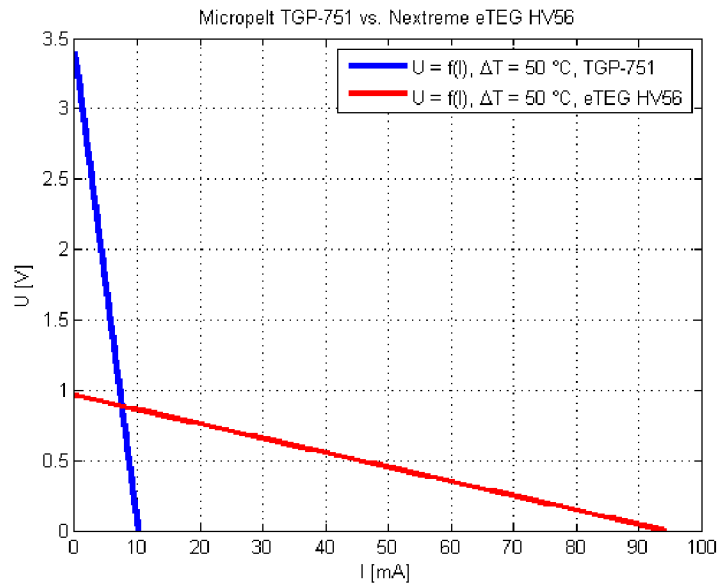
Fig. 50 V-A characteristics comparison (Micropelt TGP-751 vs. Nextreme eTEG HV56, ΔT = 50°C)

W-A characteristics in Fig. 51 shows the capability of supplying the required power to connected load. eTEG HV56 has a much better capability to do that.. Its MPP lays on 50 mA. On the other hand the voltage potential along the module is quite low (tenths of volts). Fortunately, we can conveniently use some MPPT algorithm to ensure the maximal power extraction. All the "power" characteristics were evaluated using ΔT = 50°C
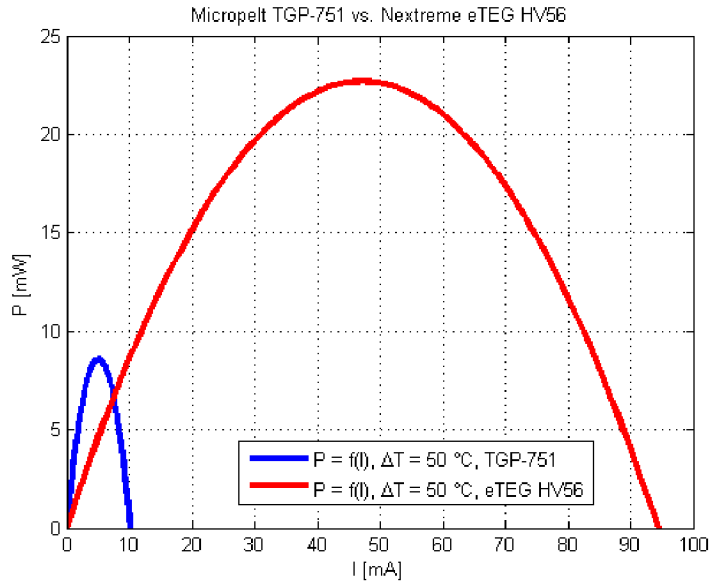
Fig. 51 W-A characteristics comparison (Micropelt TGP-751 vs. Nextreme eTEG HV56, ΔT = 50°C)

5.8 Measurement Summary

For the full identification of thermoelectric module are needed all components of Eq. 7: its thermal resistance, net Seebeck coefficient and electric resistance. The above-described measurement fully identified only the value of R_{TEM} along the whole operating temperature range. This measurement introduces a new level of quality into our models since the electrical resistance was estimated as constant given by manufacturer until this point. As it's shown in Fig. 41 and Fig. 42, R_{TEM} almost doubles when passing through the whole operating temperature range. Identification of R_{TEM} as a function of temperature is a must in the practically useful models.

The Seebeck Effect is another very important parameter for the identification of TEM. Its value can be approximately obtained from the-open circuit voltage. However the Seebeck effect obtained as a slope of Fig. 37 reaches just 65 % of datasheet value. Only two options are possible: imperfection in measurement or excessive expectations of manufacturer.

Finally, the measurement errors should be mentioned. Various errors can occur when performing these "indicative" measurements with MEMS devices and disproportionately larger measurement methods. For the precise determination of thermoelectric properties should be employed methods such as Harman probe measurement, infrared microscopy, et [27], [28]c. The largest expected error and challenge lies in the placing of Pt100 sensors to measure the exact temperature difference on such a device.

6 System-level Design

"Each system is unique. However, by capitalizing on similarities we can reduce the time, effort, and cost for some or all of them, and thus the quest for formalized design methods becomes more attractive." (Harold Chestnut)

The key requirements for the design and development of TEG were in chapter 2 set as follows:

- supplied system voltage: 3.3 V;
- supplied application power consumption: 100 mW (corresponds to current consumption about 30 mA);
- continuous operation time: 30 min;
- operating temperature range: -50 °C to +85 °C.

In Fig. 52 is depicted the simplified system diagram of supplied application along with TEG. The supplied application is data acquisition and processing from a reluctance wheelspeed sensor. This sensor is in its physical principle active and thus doesn't require any power supply instead of data acquisition and processing. The supplied circuitry consist of filter and comparator which transfers the input signal form sensor to square wave. The following block is some evaluation logic which evaluates the actual state of turbine and sends data to the output. The overall system is critical for the control of turbine or an aircraft. Therefore the utilization of thermal energy harvesting for uninterruptible power supply is considered.
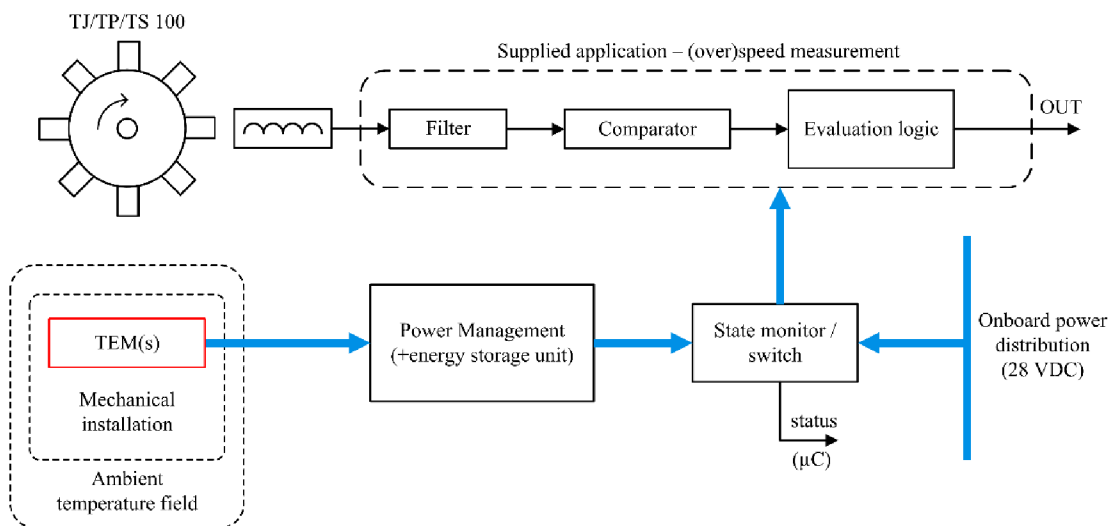
Fig. 52 Supplied application under consideration – the (over) speed measurement of TJ/TP/TS100 turbine

TEG-part of Fig. 52 consists of thermoelectric module (or modules) interacting through the mechanical installation with ambient environment – temperature field outside and inside the engine bay. Electric energy from TEM is delivered to power management with energy storage unit. This block is of high importance. It has an interface role between TEM and supplied application. Energy from the TEM is accumulated in energy storage element. Energy from

thermoelectric generator is used only if the state monitor finds some failure in the on-board power distribution. Then the switch ensures flow of energy from thermoelectric generator to supplied application.

The TJ00 jet turbine with JECU encapsulated in engine bay as shown in Fig. 53. As the JECU device is placed close to the intake air flow, the first considerations led to cooling of cold side through the forced convection from air intake.
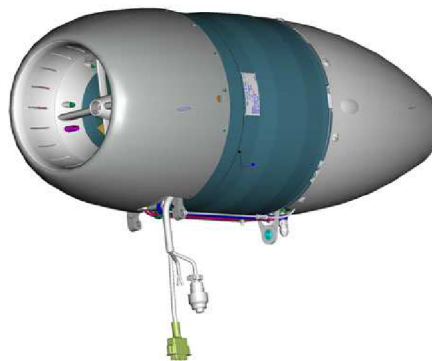
Fig. 53 TJ100 encapsulated in engine bay

Preliminary analyses shown the two prospective spots for placing the TEG. These spots are market as "spot A", "spot B" in Fig. 54. Spot B needs the additional heatsink for the heat dissipation from the JECU box to the ambient environment. In spot B, the hot side of generator is placed on the JECU box and the cold-side temperature is ensured by the natural convection to the ambient environment outside the engine bay. Spot A was rejected at the beginning of design process. Thermal camera analyses shown, that the intensive intake flow to the turbine is extensively heating up the turbine inlet. Temperature of the inlet wall is higher than the temperature of JECU. The only possible solution close to JECU is therefore on the spot B.
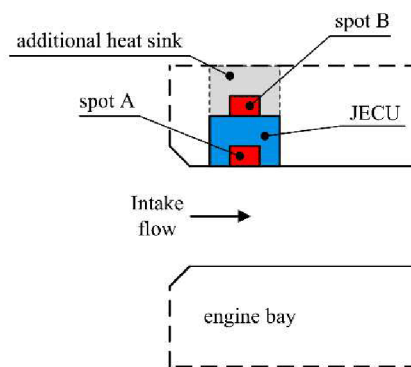
Fig. 54 Placing of TEG on the TJ100 turbine – prospective spots

Two different thermal networks were proposed for the application of TEG on the spot B. In the first one are utilized eTEG HV56 modules. The second one uses TGP-751 which is slightly less challenging in the terms of mounting ant mechanical integration. On the other hand each TGP-751 provide significantly less power then eTEG HV56. Proposed thermal networks are depicted in Fig. 55.
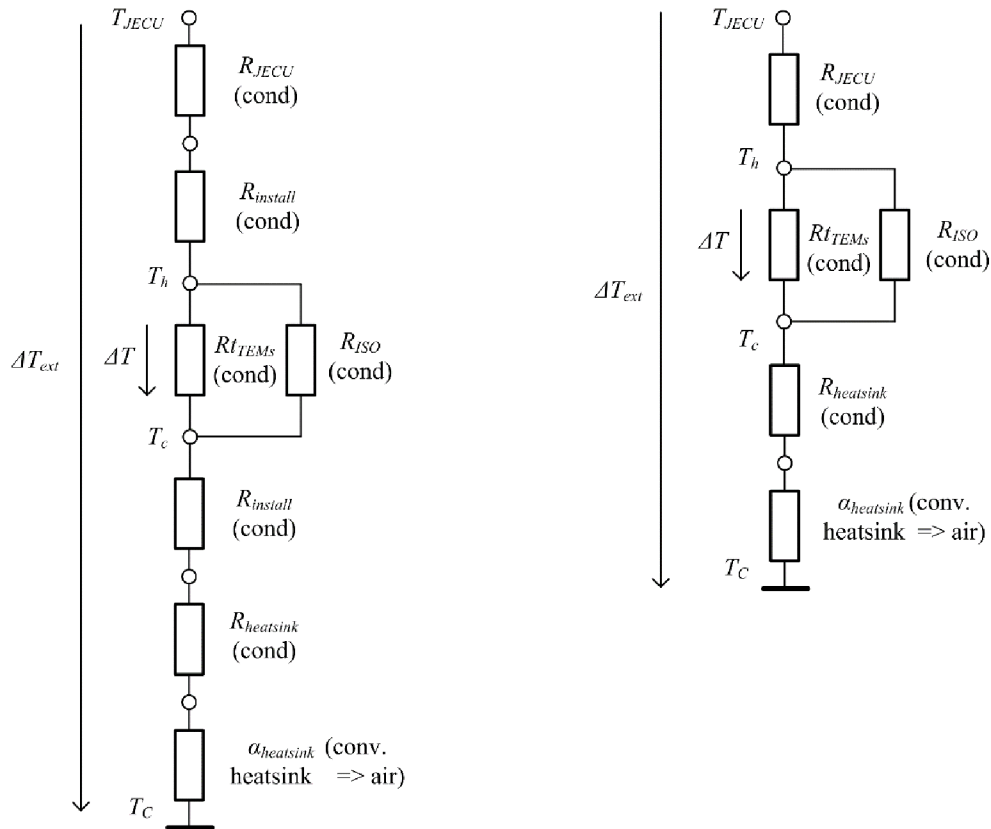
Fig. 55 Thermal networks of TEGs based on Nextreme eTEG HV56 (left) and Micropelt TGP-751 (right)

Thermal network on the left belongs to Nextrem eTEG HV56. These modules are tiny and difficult to manipulate. Thus some special aluminium adapters are necessary to accommodate these TEMs into the TEG internal structure. These aluminium adapters are denoted as $R_{install}$. Other components of thermal network are common in the both cases:

- T_{JECU} – temperature of JECU (temperature source);
- R_{JECU} – thermal resistance of path JECU-TEM;
- R_{TEM} – thermal resistance of TEM;
- $R_{heatsink}$ – thermal resistance of heat sink;
- $\alpha_{heatsink}$ – convective heat transfer coefficient to ambient air;
- ($R_{install}$) – thermal resistance of adapters for eTEG HV56;
- T_c – cold-side temperature (ambient air according to a proper flight level).

An initial idea for thermoelectric part of TEG is a connection of 1-4 TEMs to serial combination to obtain the sufficient power level for the supplied application. The higher number of MEMS TEMs would be economically disadvantageous. For the first estimation of parameters for the thermoelectric generator for JECU was used the worst-case scenario [6]. This approach is used very often when there is no further knowledge about the exact temperature fields, heat flux, etc. Input parameters were set "as bad as usually are".

6.1 Power Management Concept

The main tasks set in design of the power management electronics include the impedance matching known as Maximum Power Point Tracking (MPPT), power conditioning, interconnection with energy storage element and self-diagnostics. Proposed TEG should provide tens of milliwatts of the electric power on the voltage level of 3.3 V. Various serial/parallel/serial-parallel combinations of 1-4 TEMs will be tested consequently with a boost or buck boost converter.

The basic concept of power management for the proposed TEG is shown in Fig. 56. Blue lines are denoted as electric energy flows. Blocks are representing the detachable subsystems of the technology demonstrator.
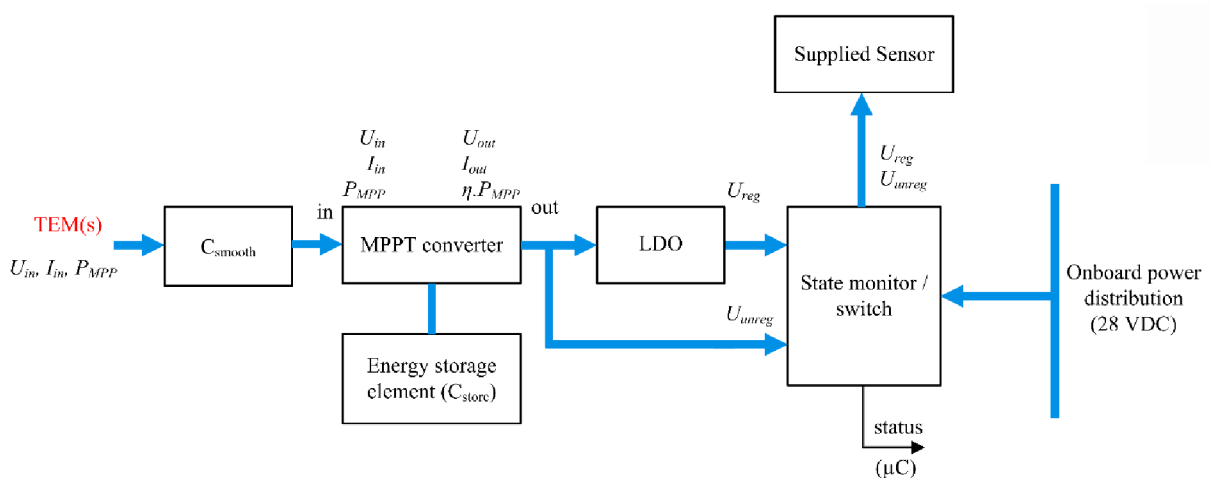
Fig. 56 Concept of power management for proposed TEG

The power output from thermoelectric module (or modules) enters the power management through the C_{smooth} capacitor. This capacitor reduces the input voltage ripple. C_{smooth} also has a positive effect on power converter stability. Maximum power point tracking is implemented as a boost or buck-boost converter. Topology will depend on the exact input voltage on the final application. The particular ICs under consideration for Nextreme eTEG HV56 modules include TI bq25504 and ST SPV1040. These ICs are depicted in their typical operation scheme in Fig. 58 resp. Fig. 59.

Another part of thermoelectric generator circuitry are LDOs. Low dropout regulators are not required in all the applications. LDOs are designed for providing the voltage references and supply voltage for critical devices. Many such a devices have an integrated LDOs in their own structure. LDOs are very frequently provided at some pins of energy harvesting electronics ICs (e.g. form Linear Technology).

State monitor / switch acts as an observer of airplane onboard power distribution. While it goes to failure state, the energy harvesting circuit is asked for operation.

The energy storage unit will be based on Supercapacitors, as discussed in chapter 4. As can be seen in Fig. 57, supercapacitors are the bottleneck of the proposed energy harvesting system. They are limited by the narrow temperature operating range. On the other hand, if considering the classic chemistry batteries, this bottleneck is even narrower.
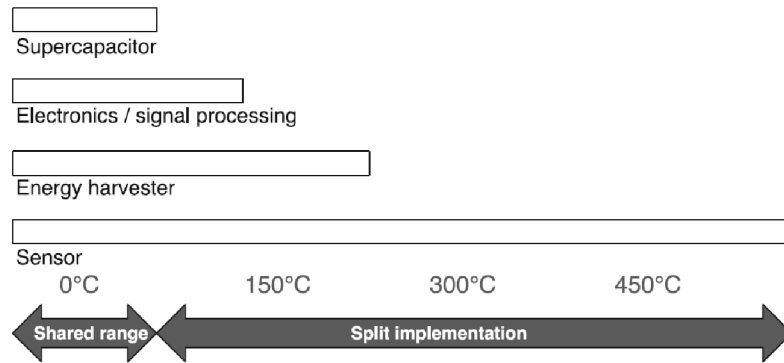
Fig. 57 Temperature is the big issue when designing the TEG for aerospace applications [8]
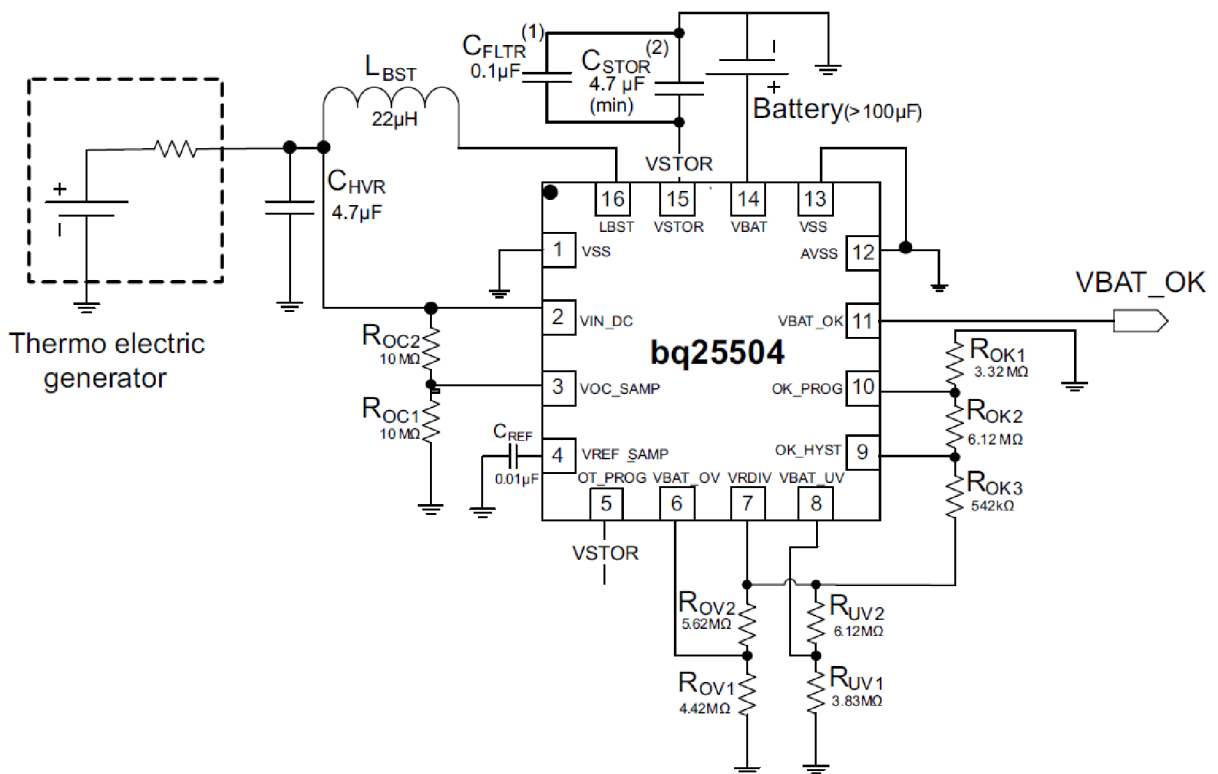
Fig. 58 Texas Instruments bq25504 – typical application circuit with thermoelectric generator [48]
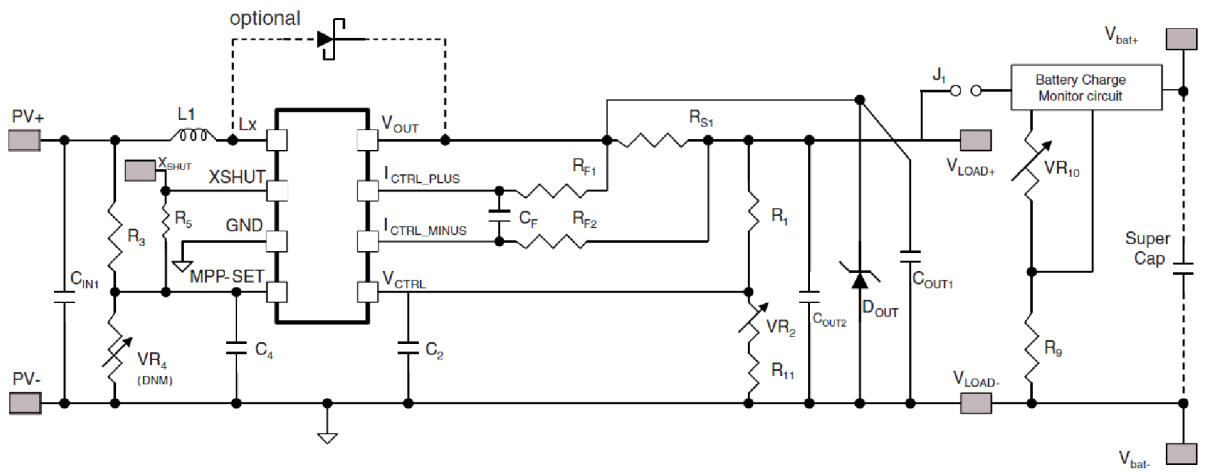
Fig. 59 ST Microelectronics SPV1040 – typical application circuit [49]

7 Modelling

"Knowledge about the process being modeled starts fairly low, then increases as understanding is obtained and tapers off to a high value at the end." (Harold Chestnut)

The model of complex thermoelectric generator is implemented in MATLAB/Simulink Simscape. The model consists of interchangeable parts which can be used in any analogic issue. Thermoelectric modules implemented in Simscape can be connected thermally into any thermal network implemented in Simscape. The same goes to electric circuits. TEM as a masked subsystem is presented in Fig. 66. First sketch of the Simscape TEM model was given in [26]. Universality predisposes the presented model for the further use in energy harvesting applications. Model consists of:

- Model of thermoelectric module (TEM);
- Model of converter;
- Model of thermal network between TEM and ambient.

7.1 Model Description

As any model working with some level of abstraction, the TEG model contain several assumptions:

- 1D heatflow;
- lumped parameters model of TEM;
- thermal and electric contact resistances are negligible;
- temperature drop on the wafer of TEM is negligible - temperature on the thermocouples is equal with temperature on wafer border;
- TEM is capable of MPP operation;
- temperature differences on all the parallel TEMs in the thermal network are equal;
- thermal resistance and Seebeck coefficient are constant over the whole operating range;

Operation of TEM model is based on the following phenomena and equations:

Peltier cooling at the both sides of module:

$$Q_{Ph} = \alpha_\Sigma I T_h \qquad\qquad \textit{(Eq. 41)}$$

$$Q_{Pc} = \alpha_\Sigma I T_c \qquad\qquad \textit{(Eq. 42)}$$

Joule heating from the current passing through TEM:

$$\frac{Q_J}{2} = \frac{1}{2} R_{TEM} I^2 \qquad \qquad \textit{(Eq. 43)}$$

Seebeck effect – the rule of thermoelectric energy conversion:

$$U_{oc} = \alpha_\Sigma (T_h - T_c) \qquad \qquad \textit{(Eq. 44)}$$

Internal resistance of such a module is computed using a lookup table which replaces the function:

$$R_{TEM} = f\left(T_{avg}\right) \qquad \qquad \textit{(Eq. 45)}$$

$$T_{avg} = \frac{T_h + T_c}{2} \qquad \qquad \textit{(Eq. 46)}$$

Implementation of coupling equations is shown in Fig. 62. Lookup table is in Fig. 63.

7.2 Model Blocks

- Thermal Reference - the thermal reference point to which are related all the temperatures defined in the system.
- I. Temperature Source - ideal source of thermal energy that is powerful enough to maintain the desired temperature difference.
- I. Heat Flow Source - ideal source of thermal energy which is powerful enough to maintain the desired heat flow regardless on temperature difference along itself.
- Conductive Heat Transfer:

$$Q = k \frac{A}{D} (T_A - T_B) \qquad \qquad \textit{(Eq. 47)}$$

  where k is the material thermal conductivity, A area normal to the heat flow direction, D distance between layers, and T_A and T_B temperatures of layers.
- Convective Heat Transfer (Newton law of cooling):

$$Q = kA(T_A - T_B) \qquad \qquad \textit{(Eq. 48)}$$

  where k is the convection heat transfer coefficient, A surface area and T_A and T_B temperatures of layers.
- I. Temperature Sensor - measures the temperature difference between two defined points without any effect on a measured system. Thermal resistance of the Ideal Temperature Sensor is infinite.
- Electrical Reference - sets the point of electric ground (point with zero potential).
- Controlled Voltage Source - provides the constant voltage regardless on the current drawn by the load connected on its terminals.
- Resistor - linear resistor with V-I characteristics according to the Ohm's law

- Current Sensor - measures the current passing through the circuit. Its internal resistance is equal to zero hence has no effect on measured circuit.
- Voltage Sensor - measures the voltage drop between its terminals. Its internal resistance is infinite hence has no effect on measured circuit.
- Simulink-PS converter - allows to convert numeric values to the SimScape physical signals.
- PS-Simulink converter - allows to convert physical signals values to the numeric values.
- Solver Configuration - defines the solver settings used for simulation.

7.3 Implementation in Simscape
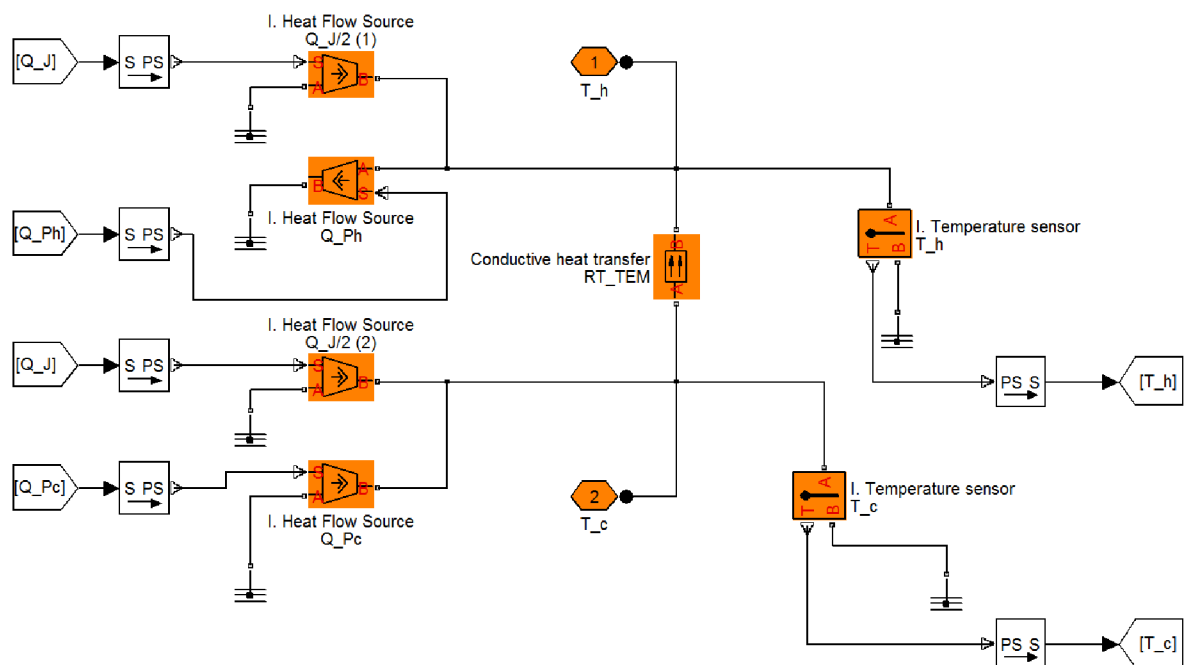
Fig. 60 Thermal part of TEM subsystem
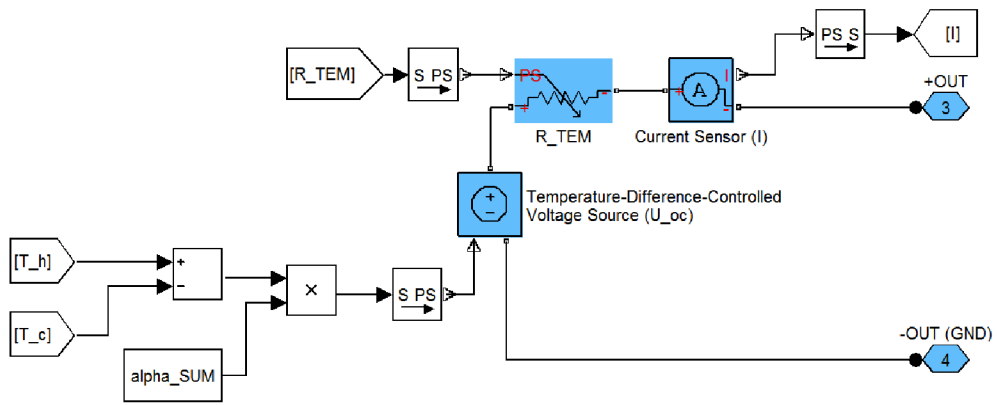
Fig. 61 Electric part of TEM subsystem
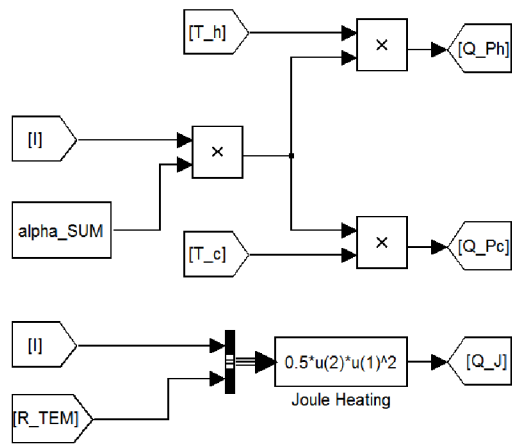
Fig. 62 Coupling equations of thermoelectric effects in TEM subsystem
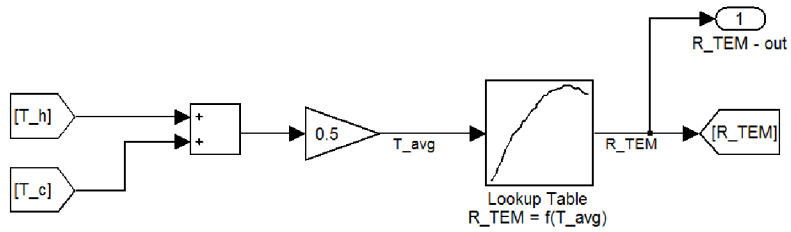
Fig. 63 Lookup table for estimation of R_{TEM} in TEM subsystem
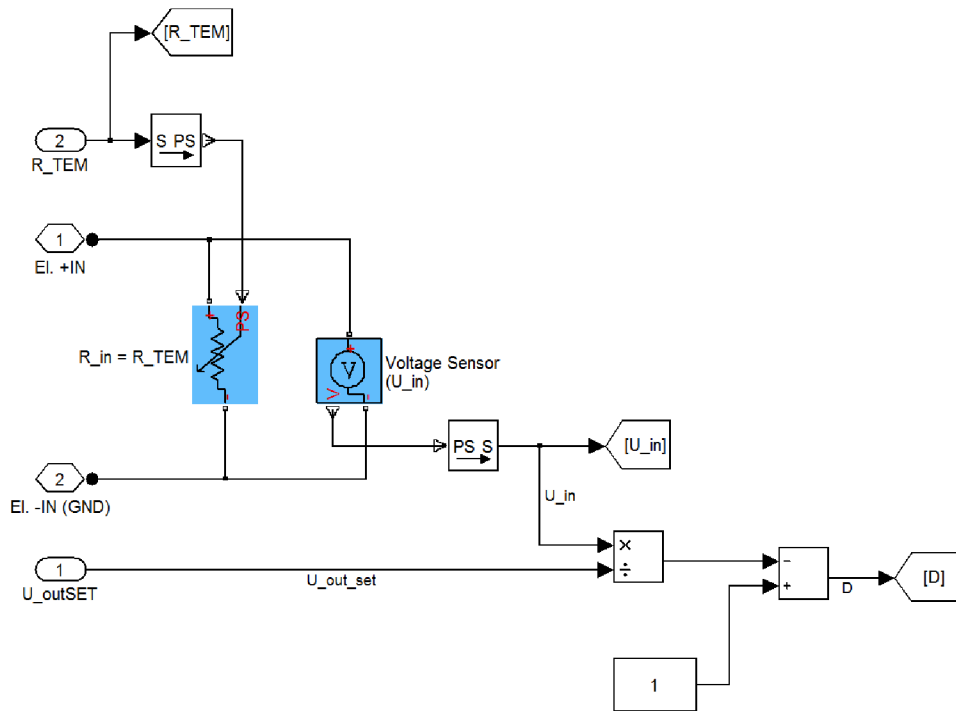
Fig. 64 Input part of boost converter subsystem
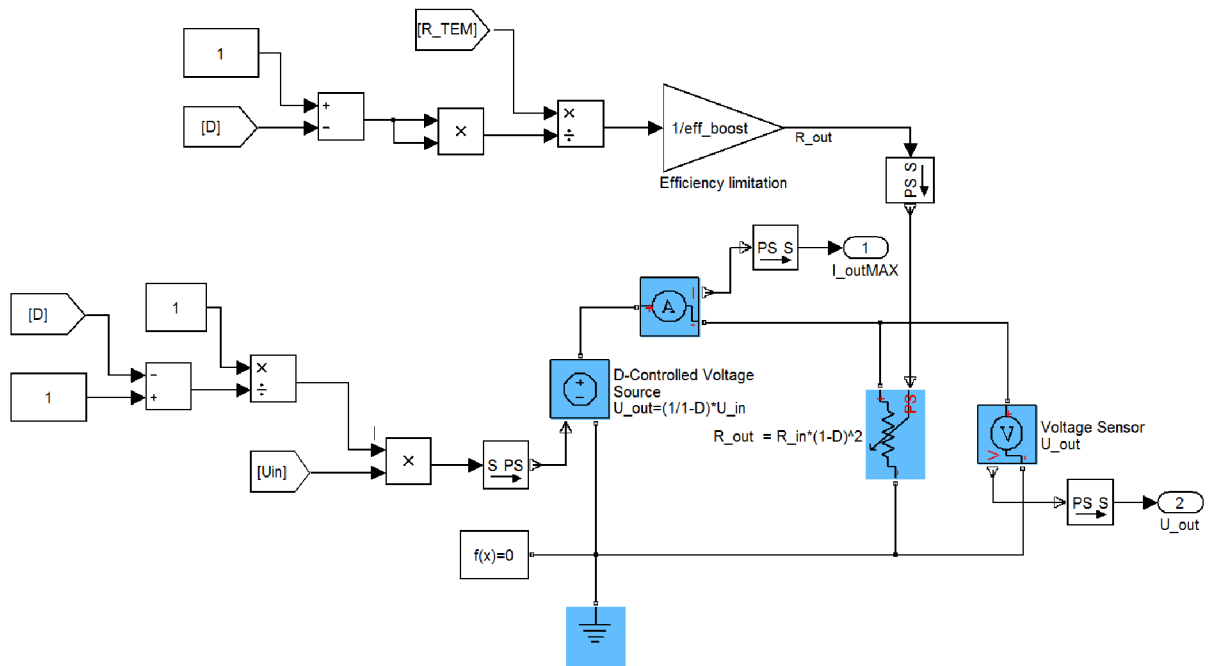
Fig. 65 Output part of boost converter subsystem

7.4 Input parameters

Input parameters to the model include:

- R_{TEM} [Ω] - thermoelectric module internal resistance
- Rt_{TEM} [W.K^{-1}] - thermal resistance of TEM
- η [-] or [%] - efficiency of converter
- α_{Σ} [V.K^{-1}] - net Seebeck coefficient
- thermal resistance of the whole heat path from
- T_H – temperature of the hot side of TEG (T_{JECU})
- T_C – temperature of the cold side of TEG

All the input parameters were taken from the measurement presented in chapter 5.

7.5 Verification

Verification of built TEM modules was performed based on comparison of measured and simulated data for the same outputs (temperature difference). TEMs were connected to a simple thermal end electric circuit according to Fig. 66/Fig. 69. Thermal input of TEM model was exposed to the same temperatures as real module under the test conditions. Results are satisfying for our required accuracy. Open-circuit voltage results perfectly match each another. Small differences between model and measured values at higher temperatures might be caused by the change of Seebeck coefficient with temperature (Fig. 70). This characteristics is not yet implemented in our simulation model. In Fig. 68 diverge the measured and simulated values for a higher temperature differecnces. This problem may be connected with the use of older data for the identification of HV56. The older data weren't measured that precisely like the new ones used in the TGP-751 model.
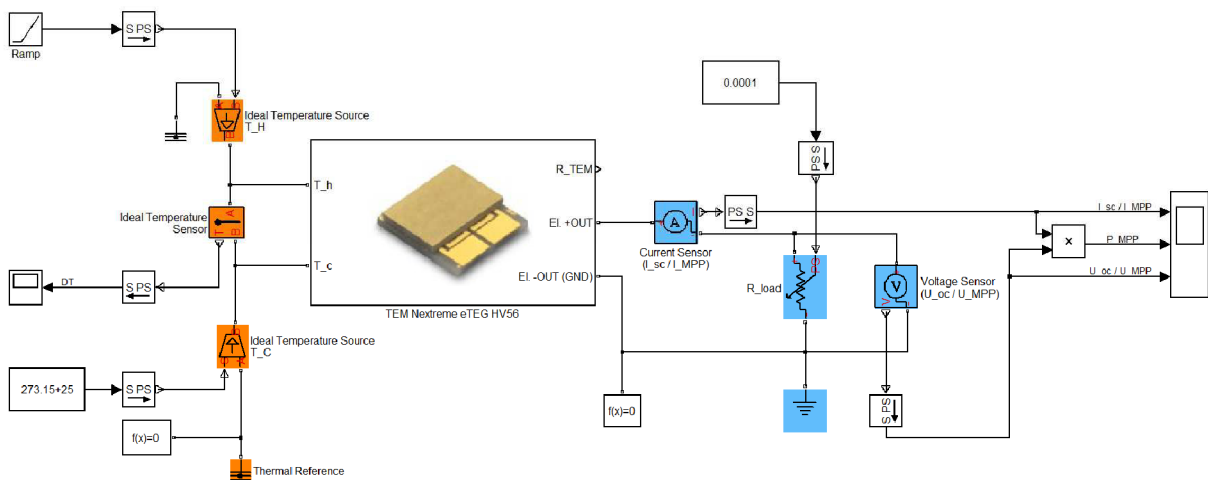
Fig. 66 Verification of eTEG HV56 model¨
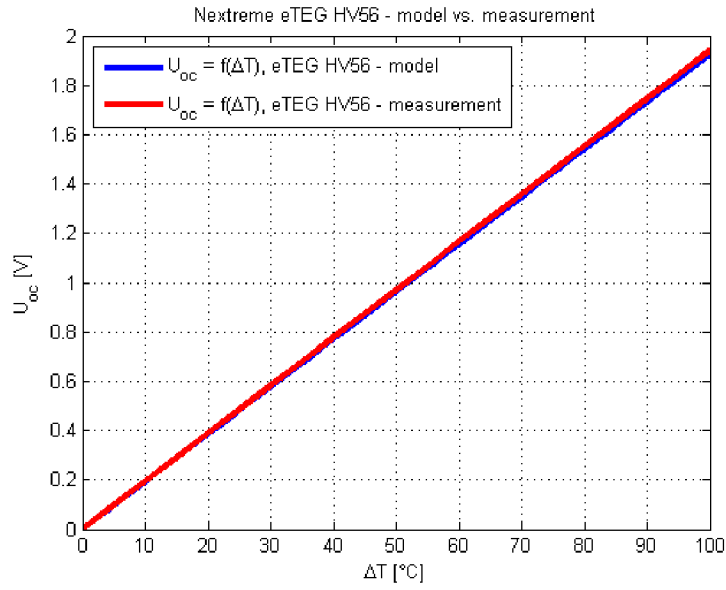
Fig. 67 Verification of eTEG HV56 model – comparison of measured and simulated open circuit voltage
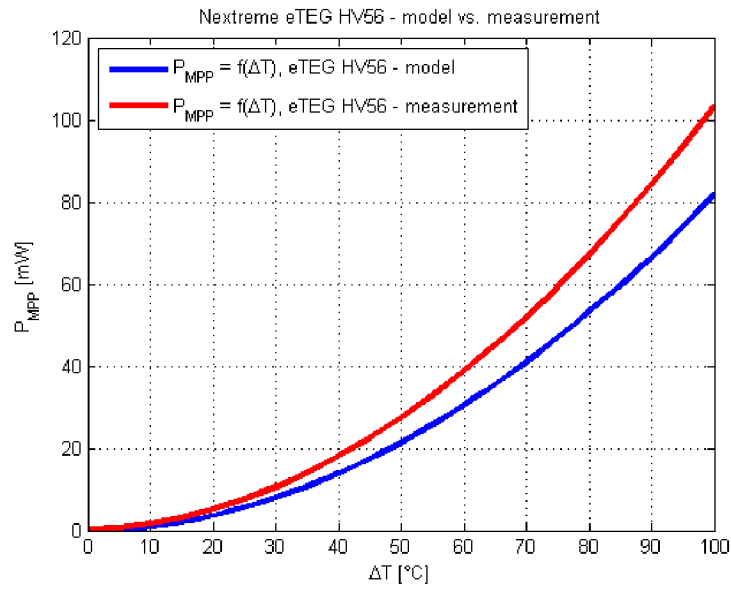
Fig. 68 Verification of eTEG HV56 model – comparison of measured and simulated power on MPP
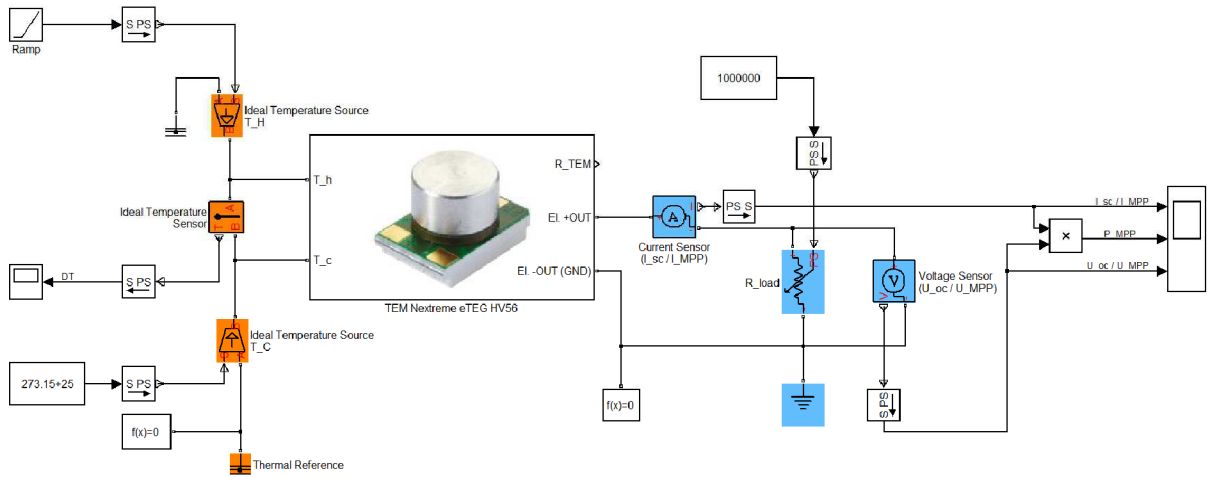
Fig. 69 Verification of TGP-751 model
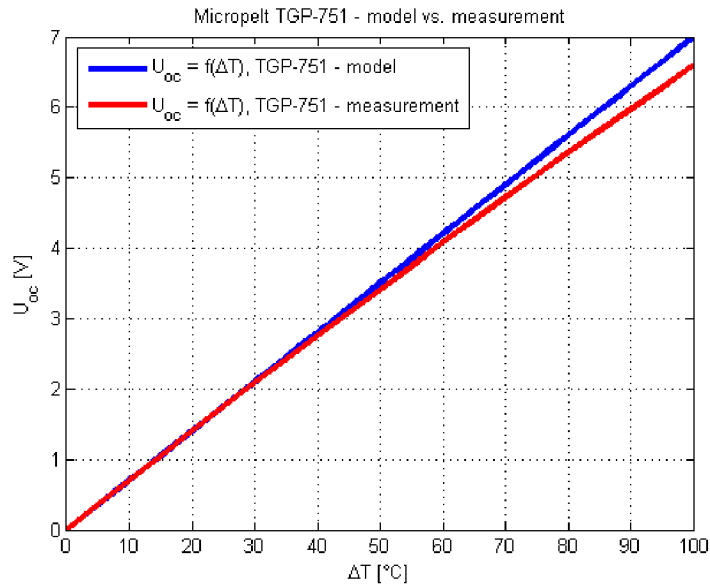
Fig. 70 Verification of TGP-751 model – comparison of measured and simulated open-circuit voltage
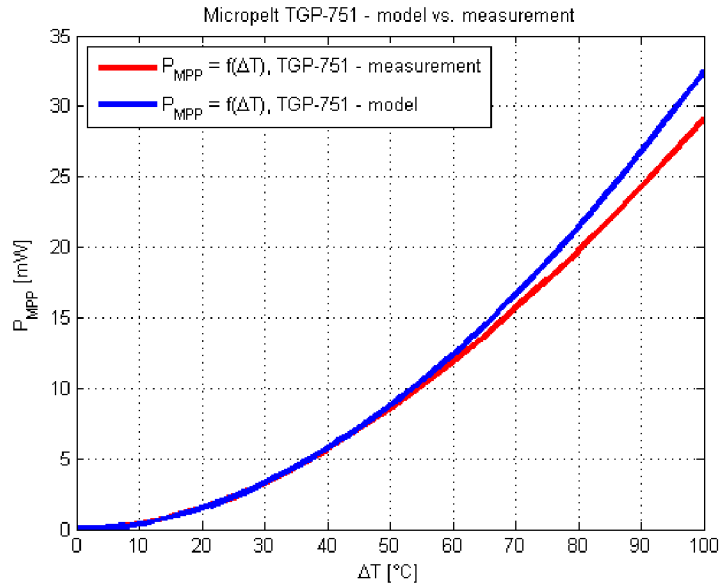
Fig. 71 Verification of TGP-751 model – comparison of measured and simulated power on MPP

Tab. 8 and Tab. 9 deal with a comprehension of experiment, model and datasheet values provided by manufacturer at several temperature difference levels. The main variations in comparable values come out with a high temperature differences. The better match between the measured and datasheet values will be the major task for the next generation of test bench.

Tab. 8 Micropelt TGP-751 – Comparison of model, measurement and datasheet values

	$\Delta T = 10\ °C$	$\Delta T = 30\ °C$	$\Delta T = 50\ °C$	$\Delta T = 100\ °C$
U_{oc} [V] (experiment)	0.705	2.088	3.405	6.6
U_{oc} [V] (model)	0.6998	2.099	3.499	6.997
U_{oc} [V] (datasheet)	1.25	3.75	5.5	11.1
I_{sc} [mA] (experiment)	2.449	7.154	11.575	22.05
I_{sc} [mA] (model)	2.134	6.254	10.01	18.54
I_{sc} [mA] (datasheet)	-	-	-	-
P_{MPP} [mW] (experiment)	0.432	3.734	9.853	36.383
P_{MPP} [mW] (model)	0.3735	3.283	8.763	32.45
P_{MPP} [mW] (datasheet)	1	8.5	-	-

Tab. 9 Nextreme HV56 – Comparison of model, measurement and datasheet values

	$\Delta T = 10\ °C$	$\Delta T = 30\ °C$	$\Delta T = 50\ °C$	$\Delta T = 100\ °C$
U_{oc} [V] (experiment)	0.194	0.582	0.97	1.94
U_{oc} [V] (model)	0.1924	0.5772	0.962	1.924
U_{oc} [V] (datasheet)	0.26	0.75	1.2	2.5
I_{sc} [mA] (experiment)	-	-	-	-
I_{sc} [mA] (model)	18.74	54.85	88.82	170.1
I_{sc} [mA] (datasheet)	24	73	115	210

P_{MPP} [mW] (experiment)	1.602	10.626	27.41	103.32
P_{MPP} [mW] (model)	0.9016	7.1915	21.36	81.84
P_{MPP} [mW] (datasheet)	1.5	17	36	130

7.6 Application on JECU

For the considered application on JECU were developed 2 models according to thermal network from Fig. 55. Into the thermal network were placed 4 thermoelectric modules. Thermoelectric modules are connected thermally in parallel and electrically n series. The alternative with Micropelt TGP-751 modules is shown in Fig. 72. Alternative for the Nextreme eTEG HV56 generator is depicted in Fig. 73. Unfortunately, the presentable results have not yet been achieved due to the major challenges with computation of the heath path resistances.
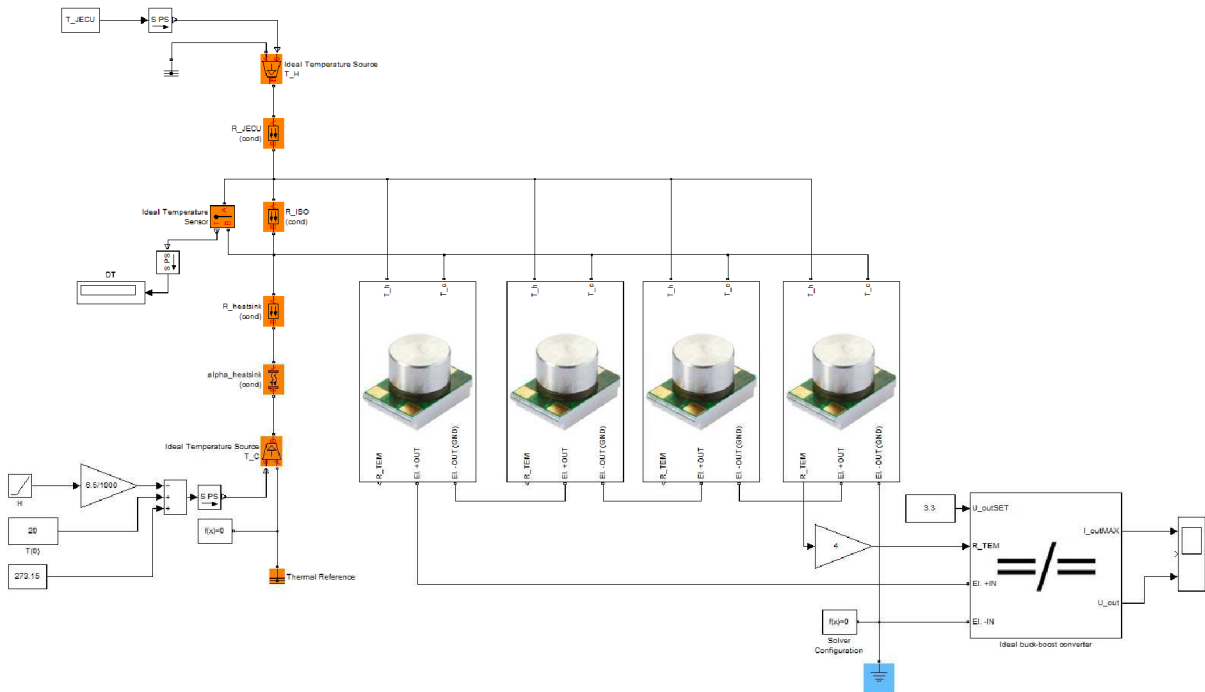
Fig. 72 – resulting simulation model of TEG for JECU with TGP-751 TEMs

Fig. 73 – resulting simulation model of TEG for JECU with Nextrem eTEGe HV56

Conclusion

"Aviation is the branch of engineering that is least forgiving of mistakes." (Freeman Dyson)

Thermoelectric generators for aerospace applications are still in their infancy. EADS Innovation Works is the only one company striding in leaps and bounds to the practical application in wireless sensor nodes.

In the previous chapters were presented the recent findings in this very perspective area of energy harvesting applications. The major attention was paid to the theoretical aspect of the design and development of thermoelectric autonomous power sources. Some basic background about the thermoelectric measurements was outlined. As an example case study have been served the specific case of thermoelectric generator for the electric power backup of turbine engine control unit (JECU). The proposed thermoelectric harvester was tailored for the use with (over)speed sensor.

The presented work mainly contributes to the experimental field of module-level thermoelectric measurements. Experimental part of the presented work have shown a new significant results. Internal resistance of MEMS thermoelectric modules was successfully measured in a wide range of operating conditions (-50 ÷ +150 °C). These characteristics are not provided by the MEMS TEM manufacturers and their further measurements have not been found in recent literature. The author's effort in the measurement and identification of MEMS thermoelectric modules will continue with their refinement.

The desired goal of this thesis was a design and development of functional technology demonstrator. This goal wasn't fully satisfied. The measurement and identification part of presented work was time consuming. Many of the measurements had to be carried out multiple times. The major problems with these measurement tasks have included the difficult manipulation with MEMS modules and the technology-related issues with glues, thermal-conductive paste, etc. The biggest issue is the mechanical installation enabling satisfactory thermal isolation of hot and cold sides of a module.

The main global challenges connected with utilization of MEMS TEMs into aerospace industry include the waiting for a utilization of new materials and improvement of their reliability. Nowadays, we have absolutely no idea about the reliability of this infant technology.

As the TEG has to be always tailored for such an application, this master's thesis will be further used as a template when developing new thermoelectric generator applications.

References

[1]   J. A. Paradiso and T. Starner, "Energy Scavenging for Mobile and Wireless Electronics," *IEEE Pervasive Comput.*, vol. 4, no. 1, pp. 18–27, 2005.

[2]   J. P. Thomas, M. a. Qidwai, and J. C. Kellogg, "Energy scavenging for small-scale unmanned systems," *J. Power Sources*, vol. 159, no. 2, pp. 1494–1509, Sep. 2006.

[3]   S. Priya and D. J. Inman, Eds., *Energy Harvesting Technologies*. New York: Springer Science+Business Media, LLC, 2009.

[4]   M. T. Penella-López and M. Gasulla-Forner, *Powering Autonomous Sensors: An Integral Approach with Focus on Solar and RF Energy Harvesting*. Dordrecht Heidelberg London New York: Springer, 2011, p. 147.

[5]   T. Becker, M. Kluge, J. Schalk, K. Tiplady, C. Paget, and U. Hilleringmann, "Autonomous Sensor Nodes for Aircraft Structural Health Monitoring," *IEEE Sens. J.*, vol. 9, no. 11, pp. 1589–1595, 2009.

[6]   M. Belleville and C. Condemine, Eds., *Energy Autonomous Micro and Nano Systems*. London/Hoboken: ISTE Ltd and John Wiley & Sons, Inc., 2012.

[7]   D. Samson, T. Otterpohl, M. Kluge, U. Schmid, and T. Becker, "Aircraft-Specific Thermoelectric Generator Module," *J. Electron. Mater.*, vol. 39, no. 9, pp. 2092–2095, Nov. 2009.

[8]   J.-M. Dilhac, R. Monthéard, M. Bafleur, V. Boitier, P. Durand-Estèbe, and P. Tounsi, "Implementation of Thermoelectric Generators in Airliners for Powering Battery-Free Wireless Sensor Networks," *J. Electron. Mater.*, vol. 43, no. 6, pp. 2444–2451, Apr. 2014.

[9]   W. Ostachowicz and J. A. Güemes, Eds., *New Trends in Structural Health Monitoring*, CISM Cours. Wien Heidelberg New York Dordrecht London: Springer, 2013, p. 427.

[10]   M. R. Pearson, M. J. Eaton, R. Pullin, C. a Featherston, and K. M. Holford, "Energy Harvesting for Aerospace Structural Health Monitoring Systems," *J. Phys. Conf. Ser.*, vol. 382, p. 012025, Aug. 2012.

[11]   A. Elefsiniotis, M. E. Kiziroglou, S. W. Wright, T. T. Toh, P. D. Mitcheson, T. Becker, E. M. Yeatman, and U. Schmid, "Performance evaluation of a thermoelectric energy harvesting device using various phase change materials," *J. Phys. Conf. Ser.*, vol. 476, p. 012020, Dec. 2013.

[12]   M. E. Kiziroglou, S. W. Wright, T. T. Toh, T. Becker, P. D. Mitcheson, E. M. Yeatman, D. U. W. Gxw, F. F. Dylrqlf, and Z. Vhqvruv, "HEAT STORAGE POWER SUPPLY FOR WIRELESS AIRCRAFT SENSORS," in *PowerMEMS 2012*, 2012, vol. 1, pp. 7–10.

[13] A. Elefsiniotis, T. Becker, and U. Schmid, "Thermoelectric Energy Harvesting Using Phase Change Materials (PCMs) in High Temperature Environments in Aircraft," *J. Electron. Mater.*, vol. 43, no. 6, pp. 1809–1814, Nov. 2013.

[14] "Autarke flexible Monitoringeinheiten zur Überwachung technischer Systeme (AMETYST)," *EADS GmbH Innovation Works*, 2010. [Online]. Available: http://www.ametyst-projekt.de/. [Accessed: 14-May-2014].

[15] L. Janák, "Application of MEMS Technology in the Field of Thermoelectric Generators," Brno University of Technology, 2012.

[16] D. Samson, M. Kluge, T. Fuss, U. Schmid, and T. Becker, "Flight Test Results of a Thermoelectric Energy Harvester for Aircraft," *J. Electron. Mater.*, vol. 41, no. 6, pp. 1134–1137, Feb. 2012.

[17] K. Thangaraj, A. Elefsiniotis, S. Aslam, T. Becker, U. Schmid, J. Lees, C. a. Featherston, and R. Pullin, "Hybrid energy storage system for wireless sensor node powered by aircraft specific thermoelectric energy harvesting," in *Proc. of SPIE Vol. 8763*, 2013, vol. 8763, p. 876307.

[18] A. Elefsiniotis, D. Samson, T. Becker, and U. Schmid, "Investigation of the Performance of Thermoelectric Energy Harvesters Under Real Flight Conditions," *J. Electron. Mater.*, vol. 42, no. 7, pp. 2301–2305, Jan. 2013.

[19] "Division of Aerospace & Advanced Control, UNIS, a.s." [Online]. Available: www.mechsys.cz. [Accessed: 14-May-2014].

[20] "První brněnská strojírna Velká Bíteš, a.s.," 2014. [Online]. Available: http://www.pbsvb.cz/. [Accessed: 09-May-2014].

[21] "Complex Affordable Aircraft Engine Electronic Control (CAAEEC)," 2014. [Online]. Available: http://www.isvav.cz/projectDetail.do?rowId=TA02010259. [Accessed: 09-May-2014].

[22] "ESPOSA - Efficient Systems and Propulsion for Small Aircraft," 2014. [Online]. Available: http://www.esposa-project.eu/. [Accessed: 09-May-2014].

[23] Division of Aerospace & Advanced Control UNIS a.s., "Jet Engine Control Unit Datasheet," Brno, 2014.

[24] Z. Ancik, "Thermal phenomena modeling of air electronic unit," Brno University of Technology, 2010.

[25] R. Isermann, "Mechatronic systems—Innovative products with embedded control," *Control Eng. Pract.*, vol. 16, no. 1, pp. 14–29, Jan. 2008.

[26] L. Janak, Z. Ancik, and Z. Hadas, "Simulation Modelling of MEMS Thermoelectric Generators for Mechatronic Applications," in *Mechatronics 2013*, 2014, pp. 265–271.

[27]   D. . Rowe, Ed., *Thermoelectrics Handbook: Macro to Nano*. Boca Raton: Taylor & Francis Group, 2006.

[28]   J. H. Goldsmith, *Introduction to Thermoelectricity*, Springer S. Heidelberg Dordrecht London New York: Springer, 2010.

[29]   V. Leonov, "Simulation of maximum power in the wearable thermoelectric generator with a small thermopile," *Microsyst. Technol.*, vol. 17, no. 4, pp. 495–504, Feb. 2011.

[30]   R. McCarty, "Thermoelectric Power Generator Design for Maximum Power: It's All About ZT," *J. Electron. Mater.*, vol. 42, no. 7, pp. 1504–1508, Oct. 2012.

[31]   A. Montecucco, J. Siviter, and A. R. Knox, "The effect of temperature mismatch on thermoelectric generators electrically connected in series and parallel," *Appl. Energy*, vol. 123, no. March, pp. 47–54, Jun. 2014.

[32]   C. Vadstrup, E. Schaltz, and M. Chen, "Individual Module Maximum Power Point Tracking for Thermoelectric Generator Systems," *J. Electron. Mater.*, vol. 42, no. 7, pp. 2203–2208, Apr. 2013.

[33]   E. A. Man, E. Schaltz, and L. Rosendahl, "Thermoelectric Generator Power Converter System Configurations: A Review," in *11th European Conference on Thermoelectrics, Proceedings of Abstracts*, 2013, p. 94.

[34]   R. W. Erickson and D. Maksimovic, *Fundamentals of Power Electronics*. New York, Boston, Dordrecht, London, Moscow: Kluwer Academic Publishers, 2004, p. 883.

[35]   E. Macii, Ed., *Ultra Low-Power Electronics and Design*. New York, Boston, Dordrecht, London, Moscow: Kluwer Academic Publishers, 2004, p. 273.

[36]   O. Lopez-Lapena, M. T. Penella, and M. Gasulla, "A New MPPT Method for Low-Power Solar Energy Harvesting," *IEEE Trans. Ind. Electron.*, vol. 57, no. 9, pp. 3129–3138, Sep. 2010.

[37]   C. Chen, W. Hsieh, W. Lai, K. Chen, and C. Wang, "A new PWM/PFM control technique for improving efficiency over wide load range," *2008 15th IEEE Int. Conf. Electron. Circuits Syst.*, pp. 962–965, Aug. 2008.

[38]   M. K. Kazimierczuk, *Pulse-Width Modulated DC-DC Power Converters*. Chichester, West Sussex: John Wiley & Sons, Ltd., 2008.

[39]   J. Park and S. Kim, "Maximum Power Point Tracking Controller for Thermoelectric Generators with Peak Gain Control of Boost DC–DC Converters," *J. Electron. Mater.*, vol. 41, no. 6, pp. 1242–1246, Jan. 2012.

[40]   Linear Technology Corporation, "LTC3108 - Ultralow Voltage Step-Up Converter and Power Manager," 2010.

[41]   Linear Technology Corporation, "LTC3109 - Auto-Polarity, Ultralow Voltage Step-Up Converter and Power Manager," 2010.

[42]   M. Aureliano, G. De Brito, L. Galotto, L. P. Sampaio, G. De Azevedo, C. A. Canesin, and S. Member, "Evaluation of the Main MPPT Techniques for Photovoltaic Applications," *IEEE Trans. Ind. Electron.*, vol. 60, no. 3, pp. 1156–1167, 2013.

[43]   I. Laird, H. Lovatt, N. Savvides, D. Lu, and V. G. Agelidis, "Comparative Study of Maximum Power Point Tracking Algorithms for Thermoelectric Generators," in *Australasian Universities Power Engineering Conference (AUPEC'08)*, 2008, pp. Paper P–217, 1–6.

[44]   Micropelt GmbH, "TGP-751 - Thin Film Thermogenerator inside standard package," 2013.

[45]   Nextreme Thermal Solutions Inc., "eTEG HV56 Power Generator - Data Sheet," 2011.

[46]   L. E. Bell, "Addressing the Challenges of Commercializing New Thermoelectric Materials," *J. Electron. Mater.*, vol. 38, no. 7, pp. 1344–1349, Feb. 2009.

[47]   M. integrated Products, "Energy-Harvesting Charger and Protector MAX17710 - datasheet," 2009.

[48]   Texas Instruments, "bq25504 - Ultra Low Power Boost Converter with Battery Management for Energy Harvester Applications," 2012.

[49]   ST Microelectronics, "SPV1040 - High efficiency solar battery charger with embedded MPPT," 2013.

[50]   ST Microelectronics, "SPV1050 - Ultralow power energy harvester and battery charger with embedded MPPT and LDOs," 2013.

[51]   Linear Technology Corporation, "LTC3105 - 400mA Step-Up DC/DC Converter with Maximum Power Point Control and 250mV Start-Up," 2010.

[52]   AVX, "AVX BestCap Ultra-low ESR High Power Pulse Supercapacitors," 2013.

[53]   Maxwell Technologies, "Product Guide: BOOSTCAP Ultracapacitors," 2009.

[54]   Maxwell Technologies, "PC SERIES ULTRACAPACITORS datasheet," 2013.

[55]   Infinite Power Solutions, "THINERGY MEC202 datasheet," 2012.

[56]   Z. Ancik, R. Vlach, L. Janak, P. Kopecek, and Z. Hadas, "Modeling, simulation and experimental testing of the MEMS thermoelectric generators in wide range of operational conditions," vol. 8763, p. 87631M, May 2013.

[57]   D. Parthasarathy, P. Enoksson, and R. Johansson, "Prototype energy harvesting wheel speed sensor for anti-lock braking," *2012 IEEE Int. Symp. Robot. Sensors Environ. Proc.*, pp. 115–120, Nov. 2012.

Table of Figures

Table of Tables

Appendix

App. 1 – Measured Values (Nextreme HV56)

	Micropelt TGP-751	Nextreme eTEG HV56
Tavg [°C]	$R_{i,TEM}$ [Ω]	$R_{i,TEM}$ [Ω]
-50	231.0	6.937
-45	234.0	7.045
-40	245.0	7.360
-35	248.0	7.560
-30	257.0	7.923
-25	263.0	8.170
-20	269.0	8.488
-15	275.0	8.650
-10	280.5	8.910
-5	284.9	9.220
0	290.1	9.313
5	299.3	9.457
10	306.6	9.620
15	320.1	9.790
20	330.8	9.922
25	330.2	10.071
30	328.0	10.264
35	332.2	10.407
40	335.8	10.523
45	340.9	10.700
50	349.5	10.831
55	356.2	10.935
60	360.0	11.080
65	366.0	11.122
70	370.4	11.275
75	377.5	11.308
80	384.0	11.350
85	389.6	11.418
90	394.3	11.435
95	396.4	11.540
100	404.6	11.558
105	409.5	11.550
110	409.5	11.584

115	417.8	11.570
120	423.0	11.535
125	426.5	11.442
130	425.5	11.480
135	433.4	11.370
140	438.1	11.300
145	440.7	11.206
150	444.7	11.150

App. 2 – Measured Values (Micropelt TGP-751)

ΔT [°C]	U_{oc}[V]	I_{sc} [mA]	P_{MPP} [mW]	T_h [°C]	T_c [°C]	T_{avg} [°C]
5	0.350	1.217	0.106	21.0	16.0	18.5
10	0.705	2.449	0.432	28.5	18.5	23.5
15	1.044	3.733	0.974	34.5	19.5	27.0
20	1.397	4.850	1.694	41.5	21.5	31.5
25	1.740	6.057	2.635	47.5	22.5	35.0
30	2.088	7.154	3.734	53.0	23.0	38.0
35	2.419	8.352	5.051	51.0	16.0	33.5
40	2.746	9.456	6.492	57.0	17.0	37.0
45	3.079	10.623	8.177	60.5	15.5	38.0
50	3.405	11.575	9.853	66.5	16.5	41.5
55	3.741	12.552	11.739	74.0	19.0	46.5
60	4.078	13.700	13.967	81.5	21.5	51.5
65	4.400	14.716	16.188	87.0	22.0	54.5
70	4.725	15.904	18.787	89.0	19.0	54.0
75	5.037	16.730	21.067	96.5	21.5	59.0
80	5.360	17.809	23.864	103.0	23.0	63.0
85	5.669	19.062	27.016	107.0	22.0	64.5
90	5.969	20.006	29.854	110.5	20.5	65.5
95	6.277	20.997	32.950	116.0	21.0	68.5
100	6.600	22.050	36.383	122.5	22.5	72.5

App. 3 – CD